Am J Physiol Heart Circ Physiol 292: H921–H927, 2007.
First published September 29, 2006; doi:10.1152/ajpheart.00019.2006.

Evaluation of transmural distribution of viable muscle by myocardial strain profile and dobutamine stress echocardiography

Takeshi Maruo,[1] Satoshi Nakatani,[1] Yintie Jin,[2] Kazunori Uemura,[2] Masaru Sugimachi,[2] Hatsue Ueda-Ishibashi,[3] Masafumi Kitakaze,[1] Tohru Ohe,[4] Kenji Sunagawa,[2] and Kunio Miyatake[1]

Departments of [1]Cardiology and [3]Pathology, National Cardiovascular Center, and [2]Department of Cardiovascular Dynamics, National Cardiovascular Center Research Institute, Osaka, Japan; and [4]Department of Cardiovascular Medicine, Okayama University Graduate School of Medicine, Okayama, Japan

Submitted 5 January 2006; accepted in final form 27 September 2006

Maruo T, Nakatani S, Jin Y, Uemura K, Sugimachi M, Ueda-Ishibashi H, Kitakaze M, Ohe T, Sunagawa K, Miyatake K. Evaluation of transmural distribution of viable muscle by myocardial strain profile and dobutamine stress echocardiography. *Am J Physiol Heart Circ Physiol* 292: H921–H927, 2007. First published September 29, 2006; doi:10.1152/ajpheart.00019.2006.—Transmural distribution of viable myocardium in the ischemic myocardium has not been quantified and fully elucidated. To address this issue, we evaluated transmural myocardial strain profile (TMSP) in dogs with myocardial infarction using a newly developed tissue strain imaging. TMSP was obtained from the posterior wall at the epicardial left ventricular short-axis view in 13 anesthetized open-chest dogs. After control measurements, the left circumflex coronary artery was occluded for 90 min to induce subendocardial infarction (SMI). Subsequently, latex microbeads (90 μm) were injected in the same artery to create transmural infarction (TMI). In each stage, measurements were done before and after dobutamine challenge (10 $\mu g \cdot kg^{-1} \cdot min^{-1}$ for 10 min) to estimate transmural myocardial viability. Strain in the subendocardium in the control stage increased by dobutamine (from 53.6 ± 17.1 to 73.3 ± 21.8%, $P < 0.001$), whereas that in SMI and TMI stages was almost zero at baseline and did not increase significantly by dobutamine [from 0.8 ± 8.8 to 1.3 ± 7.0%, P = not significant (NS) for SMI, from −3.9 ± 5.6 to −1.9 ± 6.0%, P = NS for TMI]. Strain in the subepicardium increased by dobutamine in the control stage (from 23.9 ± 6.1 to 26.3 ± 6.4%, $P < 0.05$) and in the SMI stage (from 12.4 ± 7.3 to 27.1 ± 8.8%, $P < 0.005$), whereas that in the TMI stage did not change (from −1.0 ± 7.8 to −0.7 ± 8.3%, P = NS). In SMI, the subendocardial contraction was lost, but the subepicardium showed a significant increase in contraction with dobutamine. However, in TMI, even the subepicardial increase was not seen. Assessment of transmural strain profile using tissue strain imaging was a new and useful method to estimate transmural distribution of the viable myocardium in myocardial infarction.

myocardial infarction; strain; viability; echocardiography

IT IS WELL KNOWN that myocardial contraction has transmural heterogeneity. Several experimental studies confirmed that the subendocardium contributes greater to overall myocardial thickening than the subepicardium (6, 25). On the other hand, when a reduction of coronary blood flow occurs, a severe reduction of perfusion and kinesis occurs in the subendocardium, but only a trivial reduction can be detected in the subepicardium (5, 31). After a long period of ischemia, myocardial necrosis progresses from the endocardium to the epicardium (8, 13).

Myocardial strain reflects regional myocardial function. With the recent advancement of tissue Doppler echocardiography, myocardial strain can be obtained noninvasively (3, 33) and has been reported to be useful to quantify regional myocardial systolic function in ischemic heart disease (9, 11, 24, 29, 36). The recently developed myocardial strain imaging system provides us myocardial strain in each wall layer and shows its distribution in a form of transmural myocardial strain profile (TMSP; see Ref. 1). Thus combination of TMSP and dobutamine stress echocardiography (DSE), which has been used for the assessment of myocardial viability (18), is expected to demonstrate transmural distribution of viability. There have been no methods to visualize distribution of myocardial viability over the ventricular wall in myocardial infarction, and such method would provide important information in the clinical situation.

In the present study, to assess the transmural extent of myocardial infarction, we investigated TMSP in subendocardial and transmural myocardial infarction dog models and quantified the transmural heterogeneity of myocardial viability using myocardial strain imaging with DSE.

MATERIALS AND METHODS

Experimental subjects and settings. We used 13 mongrel dogs (weighing 27.3 ± 2.2 kg). After induction with intravenous pentobarbital sodium (25 mg/kg body wt), they were anesthetized with 2% isoflurane with oxygen. A median sternotomy was performed, the pericardium was split from apex to base, and, after the instrumentation, the edges of the pericardial incision were loosely resutured. A 5-Fr. micromanometer-tipped catheter (model MPC-500; Millar Instruments, Houston, TX) was positioned in the left ventricle through the apex to obtain peak systolic left ventricular pressure and peak positive and negative dP/d*t*. Electrocardiogram (ECG) was monitored from limb leads. Left ventricular pressure signals and ECG were digitized online. The care and use of animals was in strict accordance with the guiding principles of the American Physiological Society, and the experimental protocol was approved by the National Cardiovascular Center Committees on Animal Experiments.

Experimental protocol. A 6-Fr. sheath was placed in the right femoral artery, and an angioplasty balloon catheter was positioned in the proximal segment of the left circumflex coronary artery by the standard catheterization technique. DSE (dobutamine infusion at 10 $\mu g \cdot kg^{-1} \cdot min^{-1}$ for 10 min) was used to assess myocardial viability. At the control stage, echocardiographic and hemodynamic measurements were done before and after DSE. A subendocardial myocardial infarction was created by inflating the balloon for 90 min

Address for reprint requests and other correspondence: S. Nakatani, Dept. of Cardiology, National Cardiovascular Center, 5-7-1, Fujishiro-dai, Suita, Osaka 565-8565, Japan (e-mail: nakatas@hsp.ncvc.go.jp).

The costs of publication of this article were defrayed in part by the payment of page charges. The article must therefore be hereby marked "*advertisement*" in accordance with 18 U.S.C. Section 1734 solely to indicate this fact.

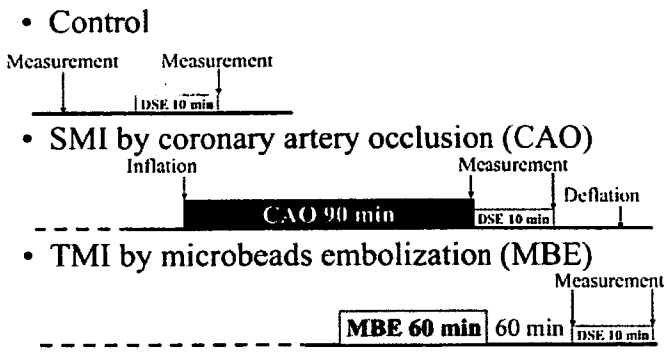

Fig. 1. Experimental protocol. DSE, dobutamine stress echocardiography; SMI, subendocardial myocardial infarction; TMI, transmural myocardial infarction.

(SMI stage; see Refs. 8 and 10), and DSE was performed during balloon inflation. After balloon deflation, 200–300 mg of latex microbeads (diameter 90 μm) were slowly injected in the same artery in 60 min to create a transmural myocardial infarction (TMI stage; see Refs. 7, 12, 15). At the TMI stage, DSE was performed 60 min after microbead embolization to complete myocardial infarction and to avoid ventricular instability to dobutamine challenge, and measurements were done before and after DSE (Fig. 1).

Ultrasound data acquisition. A commercially available ultrasound scanner (PowerVision 8000 3.5-MHz transducer; Toshiba, Tokyo, Japan) was used to obtain the epicardial left ventricular short-axis images at the level of basal and midventricle by tissue Doppler imaging. Recordings were stored in the form of digital loops of two cardiac cycles with 96–102 frames/s for subsequent analysis (33).

Tissue strain imaging. Strain is defined by the equation below and expresses the deformation of an object,

$$\text{Strain} = (L - L_0)/L_0$$

where L_0 is the length of an object before deformation and L is that after or during deformation. In echocardiography, L_0 is usually a muscle length at end diastole, and myocardial strain is used to express the deformation of local myocardial segments (4, 33).

In the present study, myocardial radial strain image was obtained from off-line analysis by using a research software TDI-Q (Toshiba; see Ref. 3). To obtain a strain image, TDI-Q software first calculates the myocardial displacement of all pixels of tissue by integrating myocardial velocity over a certain period. Because the frame rate was 96–102 frames/s, the step size for integration was 9.8–10.4 ms. Next, strain is obtained by evaluating the change of distance between pairs of two points defined on all pixels on the image by utilizing the displacement values. The distance of all two-pixel pairs at the initial time frame is equivalent to "L_0" on the above equation and set at 3 mm in this study (17). The initial time frame is set at end diastole to evaluate contraction; in other words "deformation" of the myocardium occurring in systole.

To measure local strain accurately, it is indispensable to obtain local velocity accurately. Therefore, the present myocardial strain imaging system has adopted tissue Doppler tracking and angle-correction techniques. Tissue Doppler tracking is an automatic motion tracking technique based on tissue Doppler information (30). By integrating a velocity of an indexed point on the ventricular wall known from tissue Doppler imaging, we can obtain myocardial displacement and predict the point where that point moves next. By repeating this procedure, the system can automatically track the motion of the point. With this technique, the influence of myocardial translation can be neglected. The angle-correction technique enables us to partly overcome the Doppler incident angle dependency that is inherent in Doppler echocardiography, as previous reports described (3, 26, 32). To correct the Doppler incident angle, a contraction center is set at the center of the left ventricular cavity at end systole in the left ventricular short-axis view. Next, the software automatically calculates the tissue velocity toward the contraction center (V_{motion}) by dividing the velocity toward a transducer (V_{beam}) by the cosine of the angle (θ) between the Doppler beam and the direction to the contraction center as follows:

$$V_{motion} = V_{beam}/\cos\theta$$

With the use of these two techniques, the research software TDI-Q automatically cancelled the effect of myocardial translation and angle dependency, accurately providing myocardial velocity, displacement, and strain (3). In the previously described experiments, the displacement data obtained by this method correlated with true displacement ($r = 0.99$, $P < 0.0001$; see Ref. 26).

Myocardial radial strain distribution over the myocardium is obtained as M-mode color-coded images, and the profile of distribution (TMSP) at end systole is shown as in Fig. 2. Bright color indicates high strain, and dark color indicates low strain. We obtained TMSP at basal and midinferolateral walls at end systole. We divided the myocardium into subendocardial and subepicardial half-layers by the midpoint of the myocardium at end systole. Mean strain values in the subendocardial half-layer and in the subepicardial half-layer were calculated by averaging strain values over each layer.

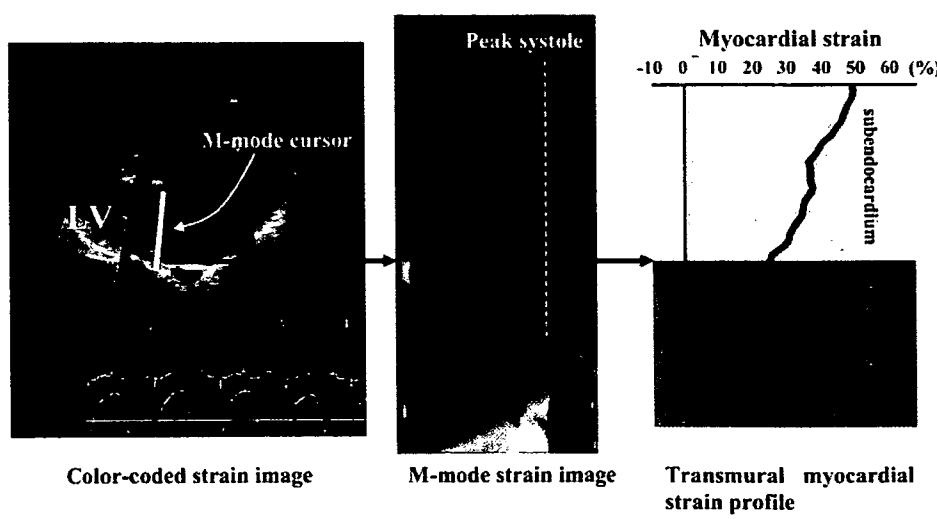

Fig. 2. Color-coded strain imaging, M-mode strain imaging, and transmural myocardial strain profile imaging in the control stage. *Left*: myocardial strain imaging of the left ventricular short axis at end systole. Red color means myocardial thickening. A white bar indicates an M-mode cursor. *Middle*: color-coded M-mode myocardial strain imaging obtained at the left ventricular posterior wall. The subendocardium is brighter than the subepicardium, indicating that the subendocardium contracts more vigorously. *Right*: transmural strain profile at end systole. The strain was highest at the subendocardium and lowest at the subepicardium, and the transmural strain showed a linear profile. LV, left ventricular wall.

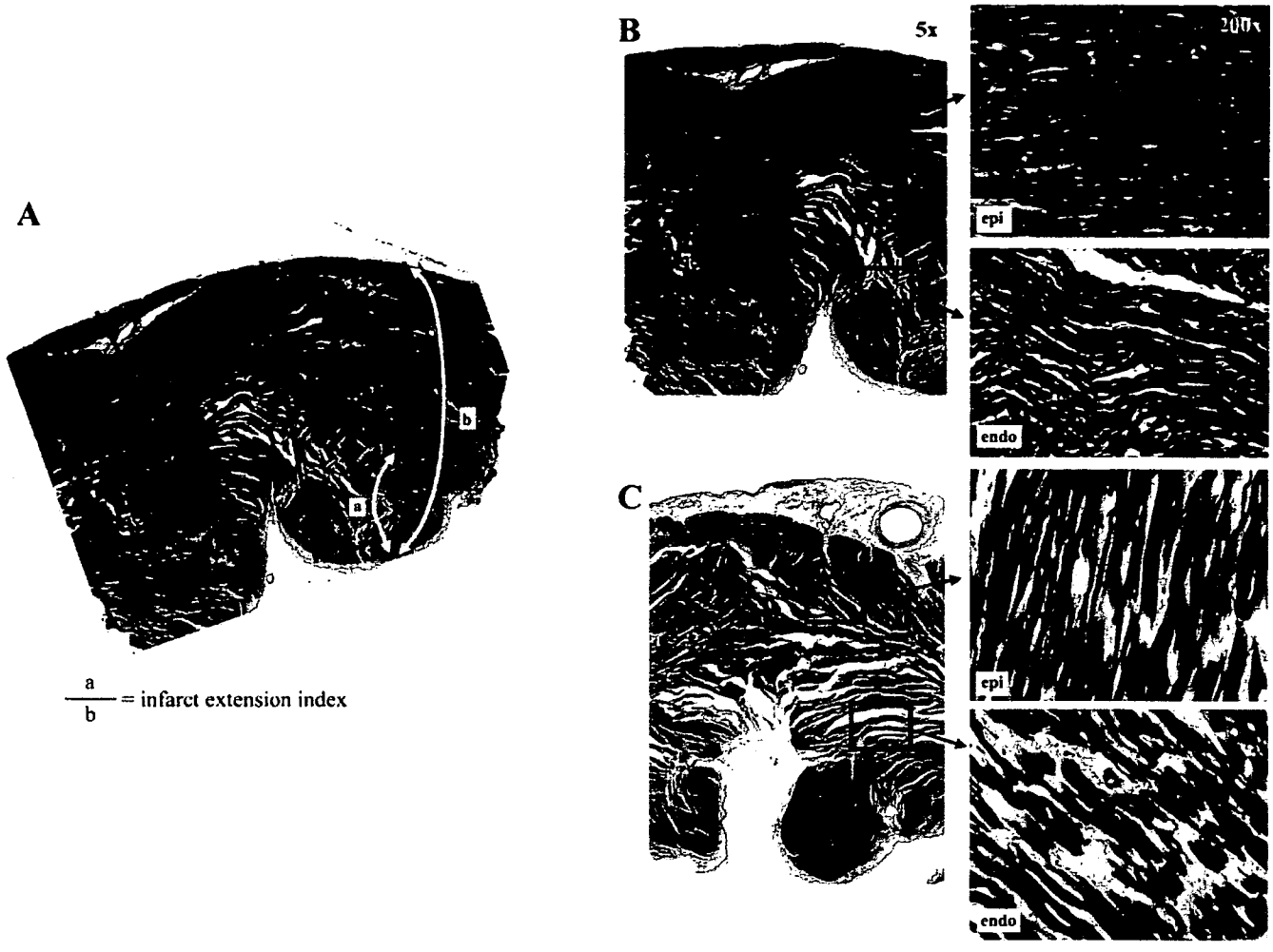

Fig. 3. *A*: determination of infarct extension index. Dotted line indicates the external limit of the infarcted zone. Examples of myocardial specimens taken after the SMI stage (*B*) and the TMI stage (*C*) stained by Masson's trichrome staining. In the SMI specimen, myocardial infarct was found only in the subendocardial layer, whereas acute ischemic changes such as wavy change or coagulation necrosis were recognized in both subendocardial and subepicardial layers in the TMI specimen. endo, Subendocardial layer; epi, subepicardial layer.

Histopathological studies. Establishment of subendocardial and transmural infarction by these techniques has been confirmed in our preliminary study and other previous studies (8, 10). We assessed the degree of extension of myocardial infarct also in the present study. At the end of the SMI stage in four dogs and the TMI stage in seven dogs, the heart was excised and cut into five to seven equally distant short-axis slices. Each slice was stained with hematoxylin-eosin and Masson's trichrome (Fig. 3). A pathologist who was blind to the experimental data examined the hearts histologically and measured the degree of infarct extension at the basal and midinferolateral walls, as previously reported (2). On each enlarged photomicrograph of the hearts, three to five transmural radii in the infarcted area were traced perpendicular to the endocardial and epicardial borders. The distance from the endocardial border to the external limit of the infarcted zone was measured and was expressed as a percentage of the distance between the endocardial and epicardial borders as an index of infarct extension, 100% being fully transmural and 0% being no infarction.

Table 1. *Hemodynamic parameters in control, SMI, and TMI stages*

	Baseline			DSE		
	Control (n = 13)	SMI (n = 11)	TMI (n = 7)	Control	SMI	TMI
HR, beats/min	133±17	128±27	129±27	149±22	134±27	150±19
LVP, mmHg	123±10*†	108±24	92±21	136±11†	132±28†	112±20
+dP/dt, mmHg/s	2,169±484*†‡	1,577±347*†	1,207±279*	4,021±979†‡	3,231±844†	2,478±1,138
−dP/dt, mmHg/s	−2,531±408*†	−1,824±606*†	−1,164±465*	−3,188±650†	−2,724±892	−2,104±526

Data are presented as means ± SD; n, no. of dogs. DSE, dobutamine stress echocardiography; SMI, subendocardial myocardial infarction; TMI, transmural myocardial infarction; HR, heart rate; LVP, peak systolic left ventricular pressure; +dP/dt, peak positive dP/dt; −dP/dt, peak negative dP/dt. $P < 0.05$ vs. DSE values (*), vs. SMI values (‡), and vs. TMI values (†).

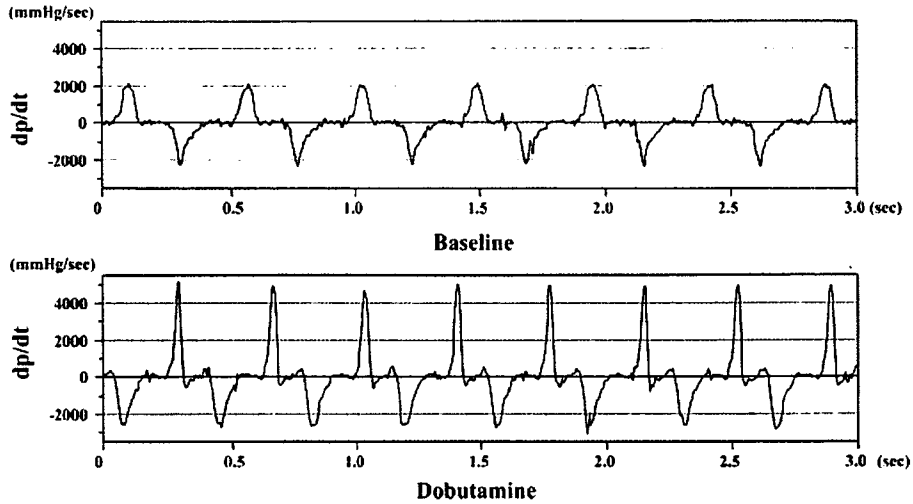

Fig. 4. dP/d*t* waveform before (*top*) and after (*bottom*) dobutamine infusion.

Reproducibility. Myocardial strain was measured by two independent observers and by one observer two times a week apart in 10 randomly selected segments to determine interobserver and intraobserver variability. The variability was assessed as the absolute difference between two measurements expressed as a percentage of their mean values. The interobserver variability was 6.5 ± 5.5 and 9.5 ± 7.5% for the subendocardial and subepicardial strains, respectively. The intraobserver variability was 7.2 ± 4.9 and 9.3 ± 3.7% for the subendocardial and subepicardial strains, respectively.

Statistical analysis. Hemodynamic data were obtained as an average of three to five consecutive beats. Statistical analyses were done with commercially available software (StatView 5.0; SAS Institute). Data are expressed as mean values ± SD. Comparisons of parameters among the stages were made by one-way ANOVA for repeated measures, followed by Scheffé's test. The Wilcoxon signed-ranks test was used to compare parameters before and after DSE. $P < 0.05$ was considered to indicate statistical significance.

RESULTS

Hemodynamic and histopathological data. Measurements were done in 13 dogs in the control stage, in 11 dogs in the SMI stage, and in 7 dogs in the TMI stage. Because of a large infarct created by the procedure, two dogs did not survive in the SMI stage and four dogs in the TMI stage. The absolute value of peak systolic left ventricular pressure and peak positive and negative dP/d*t* decreased gradually with the advancement of the stage. However, heart rate showed no significant changes. Both positive and negative dP/d*t* significantly increased in response to dobutamine administration (Table 1 and Fig. 4).

The degree of infarct extension was assessed at 14 sites from 4 dogs after the SMI stage and at 20 sites from 7 dogs after the TMI stage. The infarct extension index was 24.9 ± 7.8% for the SMI stage and 76.1 ± 9.9% for the TMI stage. Typical examples of the histopathological findings for both subendocardial and transmural infarcts are shown in Fig. 3.

Strain value in each stage. Myocardial strain was obtained at 25 segments in the control stage, at 20 segments in the SMI stage, and 11 segments in the TMI stage. Figure 5 shows representative TMSPs in each stage. In the control stage, myocardial strain was highest in the subendocardium and declined linearly toward the subepicardium. After DSE, TMSP

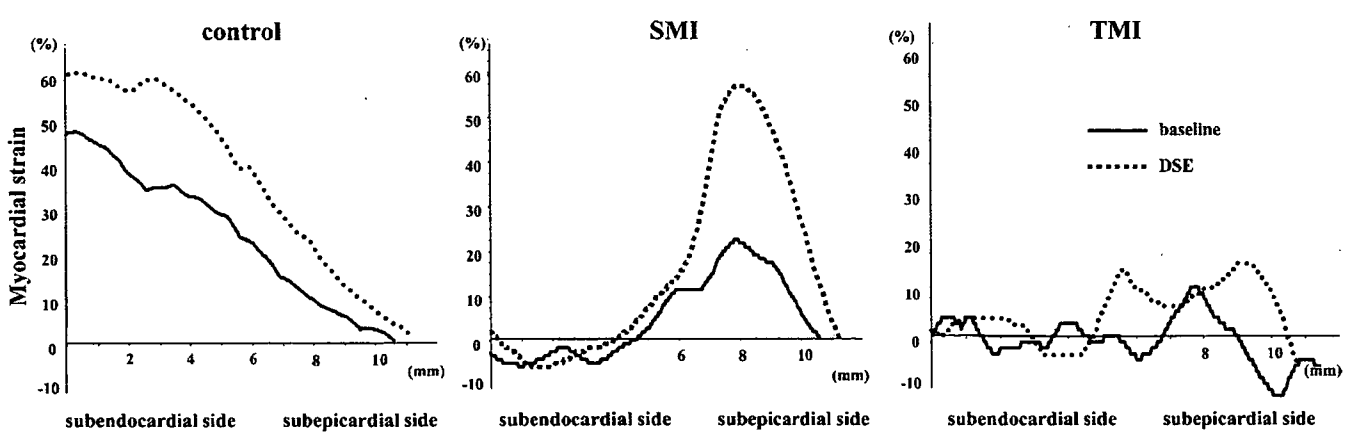

Fig. 5. Transmural myocardial strain profile before (solid lines) and after (dashed lines) dobutamine administration in each stage. *Left*: control stage. The profile was highest at the subendocardium and lowest at the subepicardium. With dobutamine administration, overall transmural myocardial strain increased. *Middle*: SMI stage. Myocardial strain at the subendocardium significantly decreased. With dobutamine administration, myocardial strain at the subepicardium showed a significant increase. *Right*: TMI stage. Overall transmural myocardial strain decreased at the baseline. Even after dobutamine administration, myocardial strain showed no significant increase.

Table 2. *Subendocardial and subepicardial strain in control, SMI, and TMI stages*

	Baseline			DSE		
	Control (n = 25)	SMI (n = 20)	TMI (n = 11)	Control	SMI	TMI
Endo strain	53.6±17.1*†‡	0.8±8.8	−3.9±5.6	73.3±21.8†‡	1.3±7.0	−1.9±6.0
Epi strain	23.9±6.1*†‡	12.4±7.3*†	−1.0±7.8	26.3±6.4†	27.1±8.8†	−0.7±8.3

Data are presented as means ± SD; n, no. of dogs. Endo strain, subendocardial strain; Epi strain, subepicardial strain. $P < 0.05$ vs. DSE values (*), vs. SMI values (‡), and vs. TMI values (†).

was uniformly uplifted, indicating the enhancement of contractility. In the SMI stage, subendocardial strain was almost zero before and after dobutamine challenge. In contrast, subepicardial strain increased after dobutamine, suggesting the presence of myocardial viability in the subepicardium. In the TMI stage, TMSP was almost flat before and after DSE, showing loss of myocardial viability through whole layers (Table 2).

Figure 6 shows changes in the subendocardial and subepicardial mean strain. Strain in the subendocardial half-layer was lower in the SMI and TMI stages than in the control stage (53.6 ± 17.1 vs. 0.8 ± 8.8 and −3.9 ± 5.6%, both $P < 0.001$).

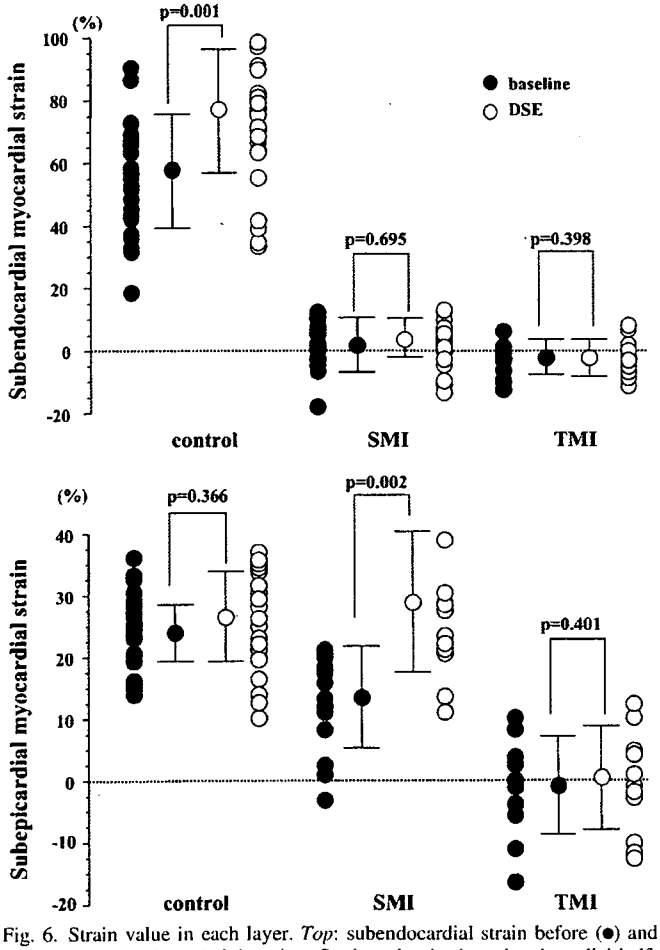

Fig. 6. Strain value in each layer. *Top*: subendocardial strain before (●) and after (○) dobutamine administration. Strain value in the subendocardial half-layer in the control stage increased with dobutamine, whereas that in the SMI and TMI stages showed no significant increase. *Bottom*: subepicardial strain before (●) and after (○) dobutamine administration. Strain value in the subepicardial half-layer in the SMI stage showed a significant increase. It showed no significant increase in the TMI stage.

There were no significant differences in the subendocardial strain between the SMI and TMI stages [P = not significant (NS)]. Strain in the subepicardial half-layer was lower in the TMI stage (−1.0 ± 7.8%) than that in the SMI stage (12.4 ± 7.3%, $P < 0.001$) and that in the control stage (23.9 ± 6.1%, $P < 0.001$).

Subendocardial strain in the control stage increased with DSE (53.6 ± 17.1 vs. 73.3 ± 21.8%, $P < 0.001$), whereas that in the SMI (0.8 ± 8.8 vs. 1.3 ± 7.0%, P = NS) and in the TMI stage (−3.9 ± 5.6 vs. −1.9 ± 6.0%, P = NS) showed no significant increase. Subepicardial strain in the control stage (23.9 ± 6.1 vs. 26.3 ± 6.4%, $P < 0.05$) and in the SMI stage (12.4 ± 7.3 vs. 27.1 ± 8.8%, $P < 0.005$) increased with DSE. It did not increase after DSE in the TMI stage (−1.0 ± 7.8 vs. −0.7 ± 8.3%, P = NS). Subepicardial strain after DSE showed no significant differences between the control and SMI stages (P = NS). These results showed that myocardial viability in the subepicardium was preserved in the SMI stage, whereas that in the TMI stage was lost.

DISCUSSION

In the present study, we analyzed the transmural distribution of viable muscle in myocardial infarction using echocardiography. Contraction in the subendocardium was lost and did not increase with dobutamine in either subendocardial infarction or transmural infarction models. On the other hand, subepicardial contraction was increased in subendocardial infarction but not in transmural infarction. These results showed that, with TMSP, we could quantify the transmural distribution of myocardial strain and identify the transmural differences in a local inotropic reserve in the viable and infarcted myocardium. The TMSP with DSE was useful to estimate the heterogeneity of transmural myocardial viability in SMI and TMI.

Transmural heterogeneity of myocardial viability. The left ventricular myocardium demonstrates transmural heterogeneity of strain distribution. It has been reported that, under normal circumstances, the subendocardial myocardium receives more blood flow and consumes more oxygen than the subepicardial one (20, 28, 35). Moreover, there is a transmural gradient of contractile function in the left ventricular wall, with greatest amount of thickening occurring in the subendocardial myocardium (6, 25). Clinically, these results were noninvasively confirmed in healthy subjects with tissue Doppler tracking technique (31). In the present study, strain value in the subendocardial layer was greater than that in the subepicardial layer in the control stage, being consistent with those of previous experimental and clinical studies. The linear decline pattern in TMSP was not observed in myocardial infarction. TMSP would potentially be useful for more detailed and innovative

evaluations of transmural myocardial function experimentally and clinically.

Effect of ischemia and dobutamine on transmural heterogeneity. After coronary artery occlusion, myocardial necrosis begins first in the endocardium and then progresses toward the epicardium with an increase in the occlusion time (8, 13). In our present study, we confirmed histologically that the SMI stage induced subendocardial infarction and the TMI stage induced transmural myocardial infarction. We observed continuous progression of myocardial dysfunction from the subendocardium to the subepicardium in myocardial infarction using echocardiography.

In acute animal models of reversible postischemic dysfunction and myocardial infarction, improved wall thickening during inotropic stimulation accurately differentiated reversible from fixed dysfunction and provided a better early assessment of viability than assessment of resting function alone (18). In clinical studies, contractile reserve by low-dose dobutamine was an independent predictor of functional recovery for myocardial infarction, which was superior to the other clinical criteria (23). In this experimental subendocardial infarction model, subendocardial strain showed no significant increase in response to inotropic stimulation, whereas subepicardial strain increased, indicating that the subepicardial myocardium was still viable. In the transmurally infarcted myocardium, myocardial strain of both subendocardium and subepicardium did not show significant increase. Therefore, the present method using TMSP and DSE is useful to visualize and quantify the contractile reserve and viability of both the subendocardium and the subepicardium.

Clinical implications. Because the prognosis of patients with subendocardial infarction is better than that with transmural infarction, assessment of the transmurality of myocardial necrosis and ischemia is an important clinical issue for patients with acute myocardial infarction or with chronic myocardial ischemia (22, 27). However, it has been difficult to make a diagnosis of subendocardial infarction by two-dimensional echocardiography. Some previous studies have shown that strain rate or strain echocardiography was useful to differentiate subendocardial infarction from transmural infarction (2, 34). We also obtained similar results using a new method of visualizing transmural myocardial strain distribution. Because the transmurality of necrosis is an important determinant of ultimate infarct size, its knowledge would be helpful in making therapeutic decisions for myocardial infarction (16, 34). Thus it is clinically helpful that we can quantify the transmural myocardial viability and necrosis extent. Furthermore, we could estimate the myocardial viability of each layer with DSE, enabling us to diagnose the stunned myocardium and predict myocardial functional recovery after myocardial infarction.

The present imaging system can be applied for the clinical evaluation of the various heart diseases characterized by subendocardial myocardial dysfunction such as anthracycline cardiotoxicity, syndrome X, hypertrophic cardiomyopathy, and dilated cardiomyopathy (14, 19, 21).

Study limitations. There was a possibility that some dogs in the subendocardial infarction models might develop transmural infarction. However, the 90-min ischemic period chosen for the subendocardial infarction models was similar to the previous studies, and it did result in subendocardial infarction (8, 10). In the present study, we showed histological evidence of subendocardial infarction after the SMI stage in parts of dogs. Furthermore, the difference in strain between the subendocardial and transmural infarction models was very prominent and consistent in each dog in the present study. These suggested that dogs after the SMI stage developed myocardial infarct almost only in the subendocardial layer.

We did not validate myocardial strain values using other methods, such as sonomicrometry. However, sonomicrometry is not always suitable to assess transmural distribution of myocardial strain, as shown in Fig. 5. We believe our measurement should be accurate because the displacement data obtained by our method were shown to be accurate (3, 21).

In conclusion, the quantitative analysis of transmural myocardial strain distribution could assess transmural differences in local inotropic reserve within the viable and infracted myocardium. In subendocardial infarction, the subepicardial myocardial strain showed an increase in contraction with dobutamine. However, in transmural infarction, this increase was lost. Assessment of transmural strain profile using tissue strain imaging was useful to quantify transmural distribution of the viable myocardium in SMI and TMI.

ACKNOWLEDGMENTS

We thank Yasuhiko Abe, Ryoichi Kanda, and Toshiba Corporation for providing research software assistance.

GRANTS

This work was partly supported by a Research Grant from the Ministry of Health, Labor and Welfare, Japan.

REFERENCES

1. **Chen X, Nakatani S, Hasegawa T, Maruo T, Kanzaki H, Miyatake K.** Effect of left ventricular systolic pressure on myocardial strain demonstrated by transmural myocardial strain profile. *Echocardiography* 23: 77–78, 2006.
2. **Derumeaux G, Loufoua J, Pontier G, Cribier A, Ovize M.** Tissue Doppler imaging differentiates transmural from nontransmural acute myocardial infarction after reperfusion therapy. *Circulation* 103: 589–596, 2001.
3. **Dohi K, Pinsky MR, Kanzaki H, Severyn D, Gorcsan J 3rd.** Effects of radial left ventricular dyssynchrony on cardiac performance using quantitative tissue Doppler radial strain imaging. *J Am Soc Echocardiogr* 19: 475–482, 2006.
4. **Edvardsen T, Gerber BL, Garot J, Bluemke DA, Lima JA, Smiseth OA.** Quantitative assessment of intrinsic regional myocardial deformation by Doppler strain rate echocardiography in humans: validation against three-dimensional tagged magnetic resonance imaging. *Circulation* 106: 50–56, 2002.
5. **Gallagher KP, Matsuzaki M, Koziol JA, Kemper WS, Ross J Jr.** Regional myocardial perfusion and wall thickening during ischemia in conscious dogs. *Am J Physiol Heart Circ Physiol* 247: H727–H738, 1984.
6. **Hartley CJ, Latson LA, Michael LH, Seidel CL, Lewis RM, Entman ML.** Doppler measurement of myocardial thickening with a single epicardial transducer. *Am J Physiol Heart Circ Physiol* 245: H1066–H1072, 1983.
7. **He KL, Dickstein M, Sabbah HN, Yi GH, Gu A, Maurer M, Wei CM, Wang J, Burkhoff D.** Mechanisms of heart failure with well preserved ejection fraction in dogs following limited coronary microembolization. *Cardiovasc Res* 64: 72–83, 2004.
8. **Homans DC, Pavek T, Laxson DD, Bache RJ.** Recovery of transmural and subepicardial wall thickening after subendocardial infarction. *J Am Coll Cardiol* 24: 1109–1116, 1994.
9. **Jamal F, Strotmann J, Weidemann F, Kukulski T, D'hooge J, Bijnens B, Van de Werf F, De Scheerder I, Sutherland GR.** Noninvasive quantification of the contractile reserve of stunned myocardium by ultrasonic strain rate and strain. *Circulation* 104: 1059–1065, 2001.
10. **Kim WG, Shin YC, Hwang SW, Lee C, Na CY.** Comparison of myocardial infarction with sequential ligation of the left anterior descend-

ing artery and its diagonal branch in dogs and sheep. *Int J Artif Organs* 26: 351–357, 2003.

11. **Kukulski T, Jamal F, Herbots L, D'hooge J, Bijnens B, Hatle L, De Scheerder I, Sutherland GR.** Identification of acutely ischemic myocardium using ultrasonic strain measurements. A clinical study in patients undergoing coronary angioplasty. *J Am Coll Cardiol* 41: 810–819, 2003.
12. **Lavine SJ, Prcevski P, Held AC, Johnson V.** Experimental model of chronic global left ventricular dysfunction secondary to left coronary microembolization. *J Am Coll Cardiol* 18: 1794–1803, 1991.
13. **Lowe JE, Cummings RG, Adams DH, Hull-Ryde EA.** Evidence that ischemic cell death begins in the subendocardium independent of variations in collateral flow or wall tension. *Circulation* 68: 190–202, 1983.
14. **Maier SE, Fischer SE, McKinnon GC, Hess OM, Krayenbuehl HP, Boesiger P.** Evaluation of left ventricular segmental wall motion in hypertrophic cardiomyopathy with myocardial tagging. *Circulation* 86: 1919–1928, 1992.
15. **Malyar NM, Lerman LO, Gossl M, Beighley PE, Ritman EL.** Relation of nonperfused myocardial volume and surface area to left ventricular performance in coronary microembolization. *Circulation* 110: 1946–1952, 2004.
16. **Mann DL, Gillam LD, Mich R, Foale R, Newell JB, Weyman AE.** Functional relation between infarct thickness and regional systolic function in the acutely and subacutely infarcted canine left ventricle. *J Am Coll Cardiol* 14: 481–488, 1989.
17. **Matre K, Fannelop T, Dahle GO, Heimdal A, Grong K.** Radial strain gradient across the normal myocardial wall in open-chest pigs measured with Doppler strain rate imaging. *J Am Soc Echocardiogr* 18: 1066–1073, 2005.
18. **Mercier JC, Lando U, Kanmatsuse K, Ninomiya K, Meerbaum S, Fishbein MC, Swan HJ, Ganz W.** Divergent effects of inotropic stimulation on the ischemic and severely depressed reperfused myocardium. *Circulation* 66: 397–400, 1982.
19. **Mortensen SA, Olsen HS, Baandrup U.** Chronic anthracycline cardiotoxicity: haemodynamic and histopathological manifestations suggesting a restrictive endomyocardial disease. *Br Heart J* 55: 274–282, 1986.
20. **Oh BH, Volpini M, Kambayashi M, Murata K, Rockman HA, Kassab GS, Ross J Jr.** Myocardial function and transmural blood flow during coronary venous retroperfusion in pigs. *Circulation* 86: 1265–1279, 1992.
21. **Panting JR, Gatehouse PD, Yang GZ, Grothues F, Firmin DN, Collins P, Pennell DJ.** Abnormal subendocardial perfusion in cardiac syndrome X detected by cardiovascular magnetic resonance imaging. *N Engl J Med* 346: 1948–1953, 2002.
22. **Picano E, Sicari R, Landi P, Cortigiani L, Bigi R, Coletta C, Galati A, Heyman J, Mattioli R, Previtali M, Mathias W Jr, Dodi C, Minardi G, Lowenstein J, Seveso G, Pingitore A, Salustri A, Raciti M.** Prognostic value of myocardial viability in medically treated patients with global left ventricular dysfunction early after an acute uncomplicated myocardial infarction: a dobutamine stress echocardiographic study. *Circulation* 98: 1078–1084, 1998.
23. **Pierard LA, De Landsheere CM, Berthe C, Rigo P, Kulbertus HE.** Identification of viable myocardium by echocardiography during dobutamine infusion in patients with myocardial infarction after thrombolytic therapy: comparison with positron emission tomography. *J Am Coll Cardiol* 15: 1021–1031, 1990.
24. **Pislaru C, Bruce CJ, Anagnostopoulos PC, Allen JL, Seward JB, Pellikka PA, Ritman EL, Greenleaf JF.** Ultrasound strain imaging of altered myocardial stiffness: stunned versus infarcted reperfused myocardium. *Circulation* 109: 2905–2910, 2004.
25. **Sabbah HN, Marzilli M, Stein PD.** The relative role of subendocardium and subepicardium in left ventricular mechanics. *Am J Physiol Heart Circ Physiol* 240: H920–H926, 1981.
26. **Sade LE, Severyn DA, Kanzaki H, Dohi K, Gorcsan J 3rd.** Second-generation tissue Doppler with angle-corrected color-coded wall displacement for quantitative assessment of regional left ventricular function. *Am J Cardiol* 92: 554–560, 2003.
27. **Sawada S, Bapat A, Vaz D, Weksler J, Fineberg N, Greene A, Gradus-Pizlo I, Feigenbaum H.** Incremental value of myocardial viability for prediction of long-term prognosis in surgically revascularized patients with left ventricular dysfunction. *J Am Coll Cardiol* 42: 2099–2105, 2003.
28. **Sjoquist PO, Duker G, Almgren O.** Distribution of the collateral blood flow at the lateral border of the ischemic myocardium after acute coronary occlusion in the pig and the dog. *Basic Res Cardiol* 79: 164–175, 1984.
29. **Skulstad H, Urheim S, Edvardsen T, Andersen K, Lyseggen E, Vartdal T, Ihlen H, Smiseth OA.** Grading of myocardial dysfunction by tissue Doppler echocardiography: a comparison between velocity, displacement, and strain imaging in acute ischemia. *J Am Coll Cardiol* 47: 1672–1682, 2006.
30. **Tanaka N, Tone T, Ono S, Tomochika Y, Murata K, Kawagishi T, Yamazaki N, Matsuzaki M.** Predominant inner-half wall thickening of left ventricle is attenuated in dilated cardiomyopathy: an application of tissue Doppler tracking technique. *J Am Soc Echocardiogr* 14: 97–103, 2001.
31. **Torry RJ, Myers JH, Adler AL, Liut CL, Gallagher KP.** Effects of nontransmural ischemia on inner and outer wall thickening in the canine left ventricle. *Am Heart J* 122: 1292–1299, 1991.
32. **Uematsu M, Miyatake K, Tanaka N, Matsuda H, Sano A, Yamazaki N, Hirama M, Yamagishi M.** Myocardial velocity gradient as a new indicator of regional left ventricular contraction: detection by a two-dimensional tissue Doppler imaging technique. *J Am Coll Cardiol* 26: 217–223, 1995.
33. **Urheim S, Edvardsen T, Torp H, Angelsen B, Smiseth OA.** Myocardial strain by Doppler echocardiography. Validation of a new method to quantify regional myocardial function. *Circulation* 102: 1158–1164, 2000.
34. **Weidemann F, Dommke C, Bijnens B, Claus P, D'hooge J, Mertens P, Verbeken E, Maes A, Van de Werf F, De Scheerder I, Sutherland GR.** Defining the transmurality of a chronic myocardial infarction by ultrasonic strain-rate imaging: implications for identifying intramural viability: an experimental study. *Circulation* 107: 883–888, 2003.
35. **Weiss HR, Neubauer JA, Lipp JA, Sinha AK.** Quantitative determination of regional oxygen consumption in the dog heart. *Circ Res* 42: 394–401, 1978.
36. **Williams RI, Payne N, Phillips T, D'hooge J, Fraser AG.** Strain rate imaging after dynamic stress provides objective evidence of persistent regional myocardial dysfunction in ischaemic myocardium: regional stunning identified? *Heart* 91: 152–160, 2005.

Am J Physiol Heart Circ Physiol 293: H1564–H1570, 2007.
First published May 25, 2007; doi:10.1152/ajpheart.00368.2007.

Muscarinic potassium channels augment dynamic and static heart rate responses to vagal stimulation

Masaki Mizuno,[1] Atsunori Kamiya,[1] Toru Kawada,[1] Tadayoshi Miyamoto,[1,2,3] Shuji Shimizu,[1,2] and Masaru Sugimachi[1]

[1]*Department of Cardiovascular Dynamics, Advanced Medical Engineering Center, National Cardiovascular Center Research Institute, and* [3]*Morinomiya University of Medical Sciences, Osaka; and* [2]*Japan Association for the Advancement of Medical Equipment, Tokyo, Japan*

Submitted 23 March 2007; accepted in final form 22 May 2007

Mizuno M, Kamiya A, Kawada T, Miyamoto T, Shimizu S, Sugimachi M. Muscarinic potassium channels augment dynamic and static heart rate responses to vagal stimulation. *Am J Physiol Heart Circ Physiol* 293: H1564–H1570, 2007. First published May 25, 2007; doi:10.1152/ajpheart.00368.2007.—Vagal control of heart rate (HR) is mediated by direct and indirect actions of ACh. Direct action of ACh activates the muscarinic K^+ (K_{ACh}) channels, whereas indirect action inhibits adenylyl cyclase. The role of the K_{ACh} channels in the overall picture of vagal HR control remains to be elucidated. We examined the role of the K_{ACh} channels in the transfer characteristics of the HR response to vagal stimulation. In nine anesthetized sinoaortic-denerved and vagotomized rabbits, the vagal nerve was stimulated with a binary white-noise signal (0–10 Hz) for examination of the dynamic characteristic and in a step-wise manner (5, 10, 15, and 20 Hz/min) for examination of the static characteristic. The dynamic transfer function from vagal stimulation to HR approximated a first-order, low-pass filter with a lag time. Tertiapin, a selective K_{ACh} channel blocker (30 nmol/kg iv), significantly decreased the dynamic gain from 5.0 ± 1.2 to 2.0 ± 0.6 (mean ± SD) beats·min^{-1}·Hz^{-1} ($P < 0.01$) and the corner frequency from 0.25 ± 0.03 to 0.06 ± 0.01 Hz ($P < 0.01$) without changing the lag time (0.37 ± 0.04 vs. 0.39 ± 0.05 s). Moreover, tertiapin significantly attenuated the vagal stimulation-induced HR decrease by 46 ± 21, 58 ± 18, 65 ± 15, and 68 ± 11% at stimulus frequencies of 5, 10, 15, and 20 Hz, respectively. We conclude that K_{ACh} channels contribute to a rapid HR change and to a larger decrease in the steady-state HR in response to more potent tonic vagal stimulation.

systems analysis; transfer function; muscarinic receptor; rabbit

VAGAL CONTROL OF HEART RATE (HR) is mediated by a cascade reaction to ACh release. ACh binds to M_2 muscarinic receptors and, consequently, decreases HR. However, the pathway is not simple; two different pathways mediate the ACh-induced HR decrease. The M_2 muscarinic receptors activate heterotrimeric G_i and/or G_o proteins in cardiac myocytes (18); the action of ACh is determined by the G_i protein subunits. Via a direct pathway, a G_i protein βγ-subunit activates inwardly rectifying muscarinic K^+ (K_{ACh}) channels in the sinoatrial node cells (11, 28, 35); K_{ACh} channels then exert a negative chronotropic effect by hyperpolarizing the sinoatrial node cells. On the other hand, via an indirect pathway, a G_i protein α-subunit suppresses adenylyl cyclase (12, 32); the suppression of adenylyl cyclase then decreases HR by inhibiting inward currents in the sinoatrial node cells, which are activated by cAMP or cAMP-dependent protein kinase. However, functional roles of the direct and indirect actions of ACh are not fully understood in the overall picture of vagal control of HR.

As a function in the dual control of adenylyl cyclase by G protein (12), the indirect action of ACh counteracts the G_s proteins activated by β_1-adrenergic sympathetic stimulation and relies on slower changes in intracellular cAMP levels (8). On the contrary, the direct action of ACh utilizes the faster membrane-delimited mechanisms involving K_{ACh} channels (3) and is believed to be independent of sympathetic control. Given the rapidity of vagal HR control compared with sympathetic control (2, 14, 31), we hypothesized that the direct action of ACh via K_{ACh} channels contributes to the quickness of the vagal HR control in vivo. To test this hypothesis, we used the selective K_{ACh} channel blocker tertiapin to examine the dynamic and static transfer characteristics of the HR response to vagal stimulation (7, 10, 13, 15).

The pioneering work by Yamada (34) demonstrated that the direct action of ACh via K_{ACh} channels mediates ~75% of the steady-state negative chronotropic effects relative to the maximum carbachol-induced bradycardia in the isolated rabbit heart (i.e., static HR response to vagal stimulation). However, in this study, the role of K_{ACh} channels in the dynamic HR response to vagal stimulation was not analyzed quantitatively. Because HR changes dynamically in response to daily activities, quantification of dynamic and static characteristics is equally important. For instance, information on the dynamic HR response is key to understanding the generation of HR variability. Berger et al. (2) used transfer function analysis to identify the dynamic characteristics of the HR response. Saul et al. (29) demonstrated the utility of transfer function analysis for insight into cardiovascular regulation. The present study aims to expand our knowledge of the involvement of K_{ACh} channels in dynamic HR control by the vagal system.

MATERIALS AND METHODS

Surgical preparations. Animal care was consistent with the "Guiding Principles for Care and Use of Animals in the Field of Physiological Sciences," of the Physiological Society of Japan. All protocols were reviewed and approved by the Animal Subjects Committee of the National Cardiovascular Center. Nine Japanese White rabbits (2.5–3.2 kg body wt) were anesthetized by a mixture of urethane (250 mg/ml) and α-chloralose (40 mg/ml): initiation with a bolus injection of 2 ml/kg and maintenance with continuous administration at 0.5

Address for reprint requests and other correspondence: M. Mizuno, Dept. of Cardiovascular Dynamics, Advanced Medical Engineering Center, National Cardiovascular Center Research Institute, 5-7-1 Fujishirodai, Suita, Osaka 565-8565, Japan (e-mail: m-mizuno@ri.ncvc.go.jp).

The costs of publication of this article were defrayed in part by the payment of page charges. The article must therefore be hereby marked "*advertisement*" in accordance with 18 U.S.C. Section 1734 solely to indicate this fact.

$ml \cdot kg^{-1} \cdot h^{-1}$. The rabbits were intubated and mechanically ventilated with oxygen-enriched room air. Arterial pressure (AP) was measured by a micromanometer (model SPC-330A, Millar Instruments, Houston, TX) inserted into the right femoral artery and advanced to the thoracic aorta. HR was measured with a cardiotachometer (model N4778, San-ei, Tokyo, Japan). A double-lumen catheter was introduced into the right femoral vein for continuous anesthetic and drug administration. Sinoaortic denervation was performed bilaterally to minimize changes in the sympathetic efferent nerve activity via arterial baroreflexes. Bilateral section of the cardiac postganglionic sympathetic nerves minimized any possible interaction between the vagus and sympathetic nerves. The vagi were sectioned bilaterally at the neck. A pair of bipolar electrodes were attached to the cardiac end of the sectioned right vagus for vagal stimulation. Immersion of the stimulation electrodes and nerves in a mixture of white petroleum jelly (Vaseline) and liquid paraffin prevented drying and provided insulation. Body temperature was maintained at 38°C with a heating pad throughout the experiment.

Experimental procedures. The pulse duration of nerve stimulation was set at 2 ms. The stimulation amplitude of the right vagus was adjusted to yield an HR decrease of ~50 beats/min at a stimulation frequency of 10 Hz. After this adjustment, the amplitude of vagal stimulation was fixed at 1.8–6.0 V. Initiation of vagal nerve stimulation over 1 h upon completion of surgical preparations allowed stable hemodynamics. A preliminary examination indicated that the response of HR to vagal stimulation was stable for up to 3 h in our experimental settings (10 min of dynamic vagal stimulation at 50-min intervals; data not shown).

Dynamic protocol. For estimation of the dynamic transfer characteristics from vagal stimulation to HR response, the right vagus was stimulated by a frequency-modulated pulse train for 10 min. The stimulation frequency was switched every 500 ms at 0 or 10 Hz according to a binary white-noise signal. The power spectrum of the stimulation signal was reasonably constant up to 1 Hz. The transfer function was estimated up to 1 Hz, because the reliability of estimation decreased as a result of the diminution of input power above this frequency. The selected frequency range sufficiently spanned the physiological range of interest with respect to the dynamic vagal control of HR.

Static protocol. For estimation of the static transfer characteristics from vagal stimulation to HR response, step-wise vagal stimulation was performed. Vagal stimulation frequency was increased from 5 to 20 Hz in 5-Hz increments. Each frequency step was maintained for 60 s.

The dynamic and static transfer functions from vagal stimulation to HR response were estimated under control and K_{ACh} channel blockade conditions. After the control data were recorded, a bolus injection (30 nmol/kg iv) of a selective K_{ACh} channel blocker, tertiapin (Peptide Institute, Osaka, Japan), was administered, and vagal stimulation protocols were repeated 15 min thereafter. The control data were obtained first in all animals, because the long-lasting (>2 h) effects of tertiapin (data not shown) did not permit the subsequent acquisition of control data. A >5-min interval between dynamic and step-wise stimulation protocols confirmed that AP and HR returned to baseline levels. Dynamic and step-wise vagal stimulation protocols were randomly assigned under control and K_{ACh} channel blockade conditions.

β-Adrenergic blockade protocol. A supplemental experiment was performed under β-adrenergic blockade ($n = 3$) eliminated any effect of sympathetic activity. At ~10 min after a bolus injection of propranolol (1 mg/kg iv) (22), HR and AP reached a new steady state. The dynamic and static transfer functions from vagal stimulation to HR response were estimated before and after tertiapin treatment, both under β-adrenergic blockade.

Data analysis. A 12-bit analog-to-digital converter was used to digitize data at 200 Hz, and data were stored on the hard disk of a dedicated laboratory computer system. The dynamic transfer function from binary white-noise vagal stimulation to HR response was estimated as follows. Input-output data pairs of the vagal stimulation frequency and HR were resampled at 10 Hz; then data pairs were partitioned into eight 50%-overlapping segments consisting of 1,024 data points each. For each segment, the linear trend was subtracted, and a Hanning window was applied. A fast Fourier transform was then performed to obtain the frequency spectra for vagal stimulation [$N(f)$] and HR [$HR(f)$] (4). Over the eight segments, the power of vagal stimulation [$S_{N \cdot N}(f)$], the power of HR [$S_{HR \cdot HR}(f)$], and the cross power between these two signals [$S_{N \cdot HR}(f)$] were ensemble averaged. Finally, the transfer function [$H(f)$] from vagal stimulation to the HR response was determined as follows (1, 20)

$$H(f) = \frac{S_{N \cdot HR}(f)}{S_{N \cdot N}(f)} \quad (1)$$

The transfer function from vagal stimulation to HR response approximated a first-order, low-pass filter with a lag time in previous studies (14, 21–24); therefore, the estimated transfer function was parameterized as follows

$$H(f) = \frac{-K}{1 + \frac{f}{f_C} j} e^{-2\pi f j L} \quad (2)$$

where K represents the dynamic gain (or, more precisely, the steady-state gain, in $beats \cdot min^{-1} \cdot Hz^{-1}$), f_c denotes the corner frequency (in Hz), L denotes the lag time (in s), and f and j represent frequency and the imaginary unit, respectively. The negative sign in the numerator indicates the negative HR response to vagal stimulation. The steady-state gain indicates the asymptotic value of the relative amplitude of the HR response to vagal nerve stimulation obtained in the frequency of input modulation approaching zero. The corner frequency represents the frequency of input modulation at which gain decreases by 3 dB from the steady-state gain in the frequency domain and reflects the readiness of the HR response for vagal stimulation in the time domain. The dynamic gain, corner frequency, and lag time were estimated by an iterative nonlinear least-squares regression. The phase shift of the transfer function indicates, with respect to the input signal, a lag or lead in the output signal normalized by its corresponding frequency of input modulation.

To quantify the linear dependence of the HR response on vagal stimulation, the magnitude-squared coherence function [$Coh(f)$] was estimated as follows (1, 20)

$$Coh(f) = \frac{|S_{N \cdot HR}(f)|^2}{S_{N \cdot N}(f) \cdot S_{HR \cdot HR}(f)} \quad (3)$$

Coherence values range from zero to unity. Unity coherence indicates perfect linear dependence between the input and output signals; in contrast, zero coherence indicates total independence between the two signals.

To facilitate the intuitive understanding of the system dynamic characteristics, we calculated the system step response of HR to 1-Hz nerve stimulation as follows. The system impulse response was derived from the inverse Fourier transform of $H(f)$. The system step response was then obtained from the time integral of the impulse response. The length of the step response was 51.2 s. We calculated the maximum step response by averaging the last 10 s of the step response. The 90% rise time of the step response was determined as the time required for the response to reach 90% of the maximum step response. The time constant of the step response was calculated from the corner frequency of the corresponding transfer function as follows

$$\text{time constant} = \frac{1}{2 \cdot \pi \cdot fc} \quad (4)$$

where the time constant is related inversely to the corner frequency without influence of the lag time.

The static transfer function from step-wise vagal stimulation to HR was estimated by averaging the HR data during the final 10 s of the 60-s stimulation at each stimulation frequency.

Statistical analysis. Values are means ± SD. Student's paired *t*-test was used to test differences in fitted parameters and calculated step response between control and K_{ACh} channel blockade conditions. For hemodynamic parameters, a two-way ANOVA, with drug and vagal stimulation as the main effects, was used to determine significant differences. For percent reduction from the control conditions in each parameter, one-way ANOVA was used to determine significant differences. $P < 0.05$ was considered significant.

RESULTS

Dynamic characteristics. Figure 1*A* shows typical recordings and corresponding power spectra of vagal stimulation and HR response under control and K_{ACh} channel blockade conditions. Random vagal stimulation decreased HR intermittently. Tertiapin-mediated K_{ACh} channel blockade attenuated the amplitude of the variation and the speed of the HR response to vagal stimulation. In the power spectral plot, tertiapin decreased the HR power. The decrease in the HR power was

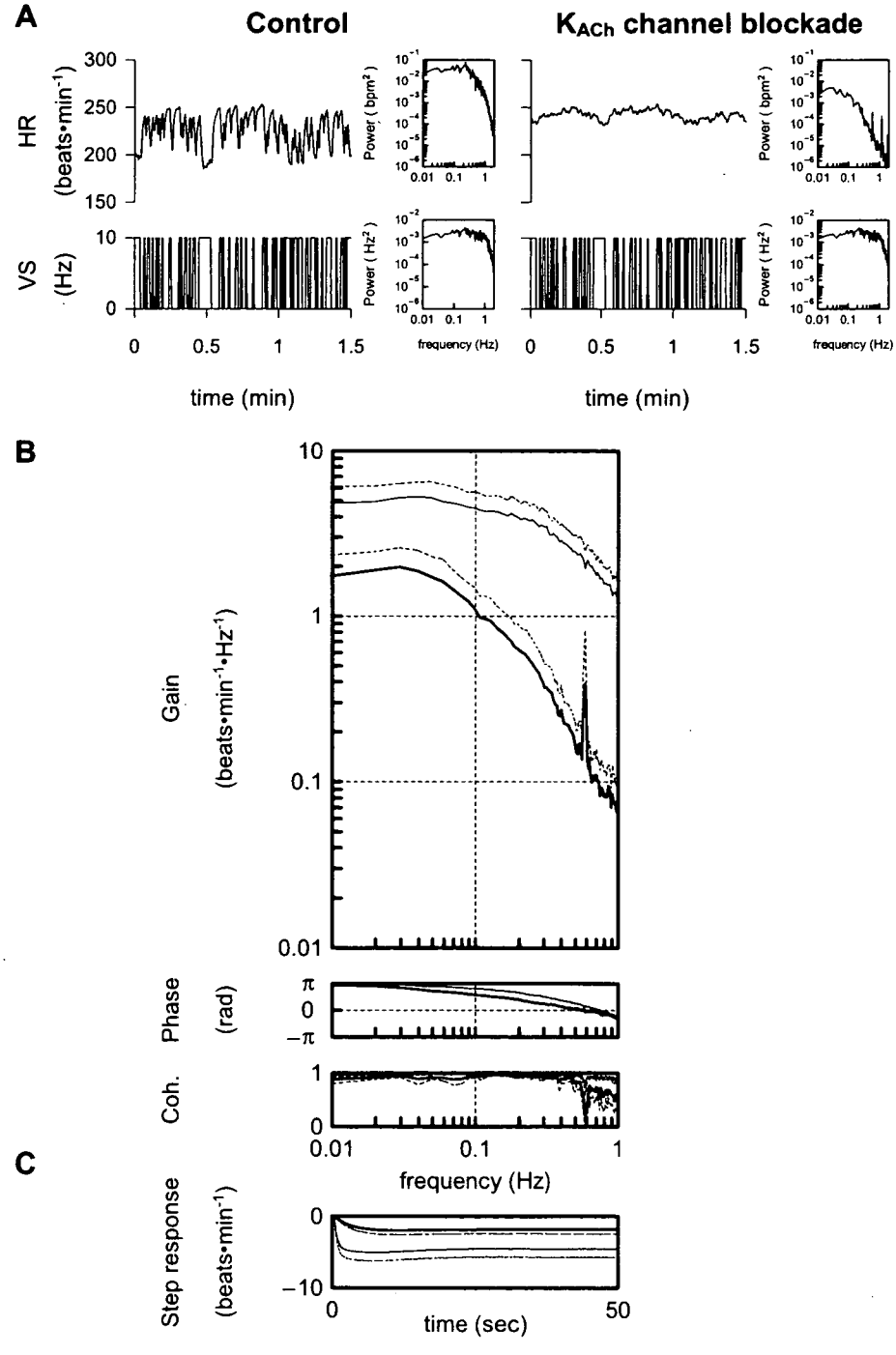

Fig. 1. *A*: representative recordings of heart rate (HR) obtained utilizing binary white-noise vagal stimulation (*top*) and corresponding vagal stimulation (VS, *bottom*). Traces were recorded before (control, *left*) and after tertiapin infusion (30 nmol/kg iv) for muscarinic K^+ (K_{ACh}) channel blockade (*right*). *Insets*: power spectra of each parameter. Tertiapin attenuated amplitude of HR variation and speed of response of HR to vagal stimulation. *B*: dynamic transfer function relating vagal stimulation to HR responses averaged from all animals (pooled data, $n = 9$). *Top*: gains; *middle*: phase shifts; *bottom*: coherence (Coh) functions. Frequency on abscissa (gain and phase) indicates frequency of input modulation, rather than stimulation frequency. *C*: calculated step response to 1-Hz tonic vagal stimulation averaged from all animals (pooled data, $n = 9$). Solid lines, means; dashed lines, SD. Thin line, control; thick line, K_{ACh} channel blockade with tertiapin (30 nmol/kg iv). Tertiapin decreased transfer gain and increased phase shift with increasing frequency, and tertiapin decreased maximum step response and slowed initial step response.

Table 1. *Effects of tertiapin infusion on AP and HR before and during dynamic vagal stimulation*

	Control	Tertiapin
AP, mmHg		
Before stimulation	82.4±20.5	77.6±20.7
During stimulation	77.9±20.0	74.8±18.6
HR, beats/min		
Before stimulation	247.3±24.7	248.1±32.7
During stimulation	212.4±22.3	231.1±25.9

Values are means ± SD (n = 9). Tertiapin was infused at 30 nmol/kg iv. AP, arterial pressure; HR, heart rate. Vagal stimulation significantly decreased HR ($P < 0.01$), but no significant effect of drug ($P = 0.28$) or interaction ($P = 0.32$) was observed by 2-way ANOVA.

more potent in the higher (>0.1 Hz) than in the lower frequency range.

Table 1 summarizes the mean values of AP and HR before and during vagal stimulation averaged from all animals. Dynamic vagal stimulation significantly decreased the mean HR ($P < 0.01$), but not the mean AP. Tertiapin did not significantly affect mean AP or HR before or during stimulation.

Figure 1*B* illustrates the dynamic transfer functions characterizing the vagal HR response averaged from all animals under control and tertiapin-mediated K_{ACh} channel blockade conditions. Gain plots, phase plots, and coherence functions are shown. Tertiapin attenuated the dynamic gain compared with the control conditions; the extent of the attenuation was greater in the higher frequency range: 63.0 ± 11.6, 74.4 ± 8.3, 93.0 ± 2.5, and 93.3 ± 3.9% at 0.01. 0.1, 0.5, and 1 Hz, respectively, as normalized to the control condition ($P < 0.01$ by ANOVA). The peak in the gain at 0.6 Hz observed during tertiapin-mediated K_{ATP} channel blockade would be caused by the artificial respiration (respiratory rate = 35–40 min^{-1}), because the low coherence value (~0.1) at 0.6 Hz indicates the independence of the input and output signals. This peak was masked by the large HR response to vagal stimulation under the control condition. The phase approached π radians at the lowest frequency and lagged with increasing frequency under the control condition; tertiapin caused the phase difference between the two conditions in the frequency range of 0.03–0.7 Hz, which disappeared at 1 Hz. The fitted parameters of the transfer functions are summarized in Table 2. Tertiapin significantly decreased the dynamic gain and the corner frequency without changing the lag time. Coherence was near unity in the overall frequency range in the control condition, whereas a decrease in the coherence function from unity was noted at >0.6 Hz with K_{ACh} channel blockade.

Figure 1*C* shows the calculated step response of HR to vagal stimulation averaged from all animals in the control condition and during K_{ACh} channel blockade. Tertiapin slowed the transient response (time constants = 0.6 ± 0.1 to 2.7 ± 0.5 s, $P <$ 0.01) and attenuated the HR response to vagal stimulation (maximum step response = −4.5 ± 1.2 to −1.8 ± 0.6 beats/min, $P < 0.01$) in the time domain. Furthermore, tertiapin significantly delayed the 90% rise time of the step response, which was calculated as an index of system readiness (1.6 ± 0.5 to 5.0 ± 1.4 s, $P < 0.01$).

Static characteristics. Figure 2*A* shows typical recordings of step-wise vagal stimulation and the HR response in the control condition and during K_{ACh} channel blockade. The step-wise vagal stimulation decreased HR in a step-wise manner. Tertiapin attenuated the static reductions of HR from the baseline HR.

Figure 2*B* summarizes changes in HR in response to step-wise vagal stimulation. The step-wise vagal stimulation significantly decreased HR with increasing stimulus frequency under both conditions. Tertiapin significantly attenuated the static reductions of HR. The attenuation of HR reduction normalized to control conditions increased with increasing stimulus frequency: 45.8 ± 21.3, 58.2 ± 17.9, 64.7 ± 14.6, and 68.0 ± 11.4% at 5, 10, 15, and 20 Hz, respectively ($P < 0.05$ by ANOVA).

β-Adrenergic blockade protocol. In the supplemental protocol (n = 3) with β-adrenergic blockade, tertiapin decreased the dynamic gain from 2.4 ± 0.6 to 1.3 ± 0.5 beats·min^{-1}·Hz^{-1} and the corner frequency from 0.23 ± 0.05 to 0.06 ± 0.02 Hz without changing the lag time (0.36 ± 0.01 vs. 0.43 ± 0.00 s). In terms of the static characteristics, tertiapin significantly attenuated the vagal stimulation-induced HR decrease by 43 ± 10, 50 ± 8, 56 ± 7, and 61 ± 8% at stimulus frequencies of 5, 10, 15, and 20 Hz, respectively.

DISCUSSION

We have quantified the role of the K_{ACh} channels by examining the transfer characteristics. The major findings in the present study are that K_{ACh} channel blockade with intravenous tertiapin administration decreased the dynamic gain and corner frequency without changing the lag time of the dynamic transfer function from vagal stimulation to HR. These findings support our hypothesis that direct action of ACh via K_{ACh} channels contributes to the quickness of the HR control in response to electrical vagal stimulation.

Effect of tertiapin on dynamic transfer characteristics. Our results indicate that K_{ACh} channels contribute to a rapid component in vagal HR control. Tertiapin slowed the dynamic HR response to vagal stimulation, since tertiapin attenuated the gain of the transfer function significantly in the high frequency range (Fig. 1*B*). Moreover, the calculated step response clearly demonstrated this point (Fig. 1*C*). Tertiapin prolonged the time constant and 90% rise time of the step response by 2.1 and 3.4 s, respectively. Since quickness is a hallmark of the vagal control of HR relative to sympathetic control, these results highlight the importance of K_{ACh} channels in the rapidity of vagal HR control. Because tertiapin did not affect the lag time (Table 2), the increase in the 90% rise time to the step response due to tertiapin (~3.4 s) may primarily reflect the slowed transient response.

Our results are consistent with and may partly explain the earlier studies in which transgenic mice were used to investigate the role of K_{ACh} channels (8, 33). Using the G protein-

Table 2. *Effects of tertiapin infusion on parameters of the transfer function relating dynamic vagal stimulation to HR*

	Control	Tertiapin
Dynamic gain, beats·min^{-1}·Hz^{-1}	5.0±1.2	2.0±0.6*
Corner frequency, Hz	0.25±0.03	0.06±0.01*
Lag time, s	0.37±0.04	0.39±0.05

Values are means ± SD. Tertiapin was infused at 30 nmol/kg iv. *$P < 0.01$ vs. corresponding control.

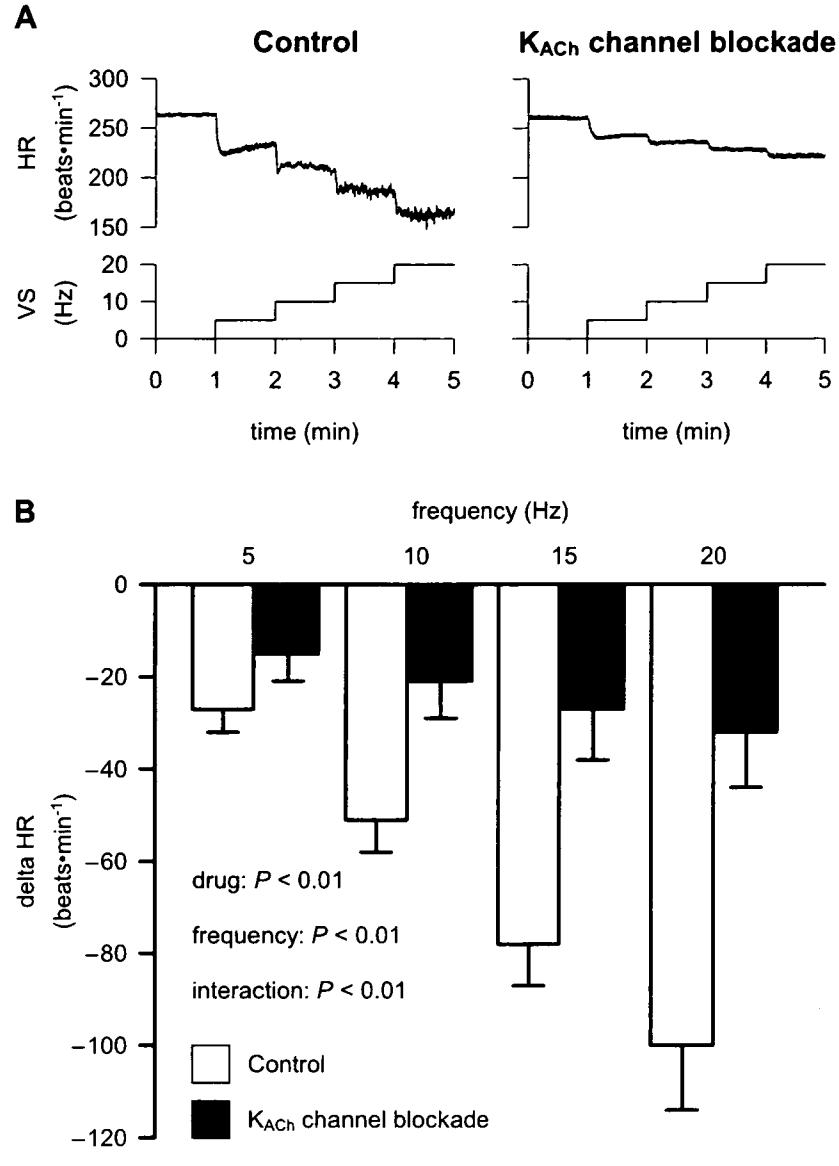

Fig. 2. *A*: representative recordings of HR (*top*) and corresponding vagal stimulation (*bottom*) obtained utilizing a step-wise stimulation. Traces were recorded before (control, *left*) and after tertiapin infusion (30 nmol/kg iv) for K_{ACh} channel blockade (*right*). K_{ACh} channel blockade attenuated amplitude of HR variation to tonic vagal stimulation. *B*: static transfer function relating step-wise vagal stimulation to HR responses averaged from all animals (pooled data, $n = 9$). Basal HR was not different between control and K_{ACh} channel blockade (see Table 1). K_{ACh} channel blockade decreases static HR response, and static reductions in bradycardic effect were greater at higher stimulation frequencies.

gated inwardly rectifying potassium (GIRK) channel family subunit GIRK4, which is a component of K_{ACh} channels (5, 16), Wickman et al. (33) indicated that the spectral power of HR was lower at 1.5–5.0 Hz, which is predominantly vagally mediated, but not at <0.4 Hz, in GIRK4-knockout than in wild-type mice. Another study using transgenic mice with a reduction in functional βγ-subunits of the G_i proteins also showed impaired vagal HR control, such as reductions in carbachol-induced bradycardia, HR variability, and baroreflex sensitivity (8). In the present study, tertiapin significantly attenuated the dynamic gain compared with the control conditions in the frequency bands from 0.01 to 1 Hz; the extent of the decreases in dynamic gain was augmented with increasing frequency of input modulation. This finding also supports the notion that K_{ACh} channels play a large part as a rapid component of vagal control of HR. Furthermore, increased phase shift due to tertiapin in the higher frequency range (0.03–0.7 Hz) would support the interpretation that the K_{ACh} channel current played an important role in the rapid HR response to vagal stimulation.

Tertiapin-mediated changes in fitted parameters of the transfer function from vagal stimulation to HR suggest that, at the postjunctional effector sites, the K_{ACh} channels play a key role in determining the dynamic properties of transduction from vagal nerve activity to HR. To quantitatively elucidate vagal and sympathetic control of HR, our research group used a transfer function analysis to examine the system characteristics. First, the transfer function from dynamic vagal nerve stimulation to HR approximated the characteristics of a first-order, low-pass filter, whereas the transfer function from dynamic sympathetic nerve stimulation to HR approximated the characteristics of a second-order, low-pass filter (14). Dynamic gain of vagal stimulation to HR was increased by concomitant sympathetic nerve stimulation (14) and pharmacologically induced accumulation of cAMP at the postjunctional effector sites (23) and decreased by high plasma norepinephrine (21). These perturbations of the indirect action of ACh did not affect the quickness of vagal HR control; i.e., neither corner frequency nor lag time was altered. On the contrary, inhibition of cholinesterase by neostigmine decreased the corner frequency

and increased the lag time (24). Taken together, these results might suggest that not only ACh kinetics at the neuroeffector site, but also the K_{ACh} channels at the postjunctional effector sites, play a key role in determining the dynamic properties of transduction from vagal nerve activity to HR.

Effect of tertiapin on the static transfer characteristics. Tertiapin attenuates the static reduction of HR in accord with the attenuation of the gain of the dynamic transfer function at the lowest frequency of input modulation. This suggests that K_{ACh} channels contribute to the static, as well as the rapid, component of vagal HR control. The relative attenuation of HR reduction increased with increasing stimulus frequency (Fig. 2*B*), suggesting that direct action of ACh in the static properties of transduction from vagus nerve activity to HR is augmented by an increase in the amount of available ACh. Although it is well established that the muscarinic response to static vagal stimulation depends on the stimulation frequency (26, 27), whether the contribution of the K_{ACh} channel pathway to the total HR response depends on the stimulus frequency remains unknown. The basal mean HR of GIRK-knockout mice (33) and transgenic mice with a reduction of βγ-subunits of the G_i proteins (8) is the same as that of wild-type mice, suggesting that K_{ACh} channels are not involved in mean HR control in the basal state. At low-to-moderate levels of vagal activity, vagal control of HR is due to changes in cAMP-modulated I_h, often referred to as "pacemaker" current (6). K_{ACh} channels might play an essential role in HR control at high levels of vagal activity.

In the present study, tertiapin decreased the HR response to vagal stimulation by ~70% of the control condition at a stimulus intensity of 20 Hz. This value is consistent with the earlier study by Yamada (34). This consistency suggested that K_{ACh} channels contribute to ~70% of the maximum negative chronotropic effects to pharmacologically and/or electronically induced vagal stimulation. However, changes in HR induced by tertiapin may have in turn affected the indirect action of ACh in the present study. Therefore, the percentage of direct vs. indirect action should be carefully interpreted.

Limitations. There are several limitations to this study. First, we did not confirm the completeness of K_{ACh} channel blockade. Kitamura et al. (15) demonstrated that tertiapin potently and selectively blocked the K_{ACh} channel in cardiac myocytes in a muscarinic receptor- and voltage-independent manner. Furthermore, Drici et al. (7) showed that tertiapin blocked K_{ACh} channels with an IC_{50} of ~30 nM with no significant effect on major currents associated with the cardiac repolarization process or atrioventricular conduction. On the basis of these studies, Hashimoto et al. (10) demonstrated that tertiapin (12 nmol/kg iv) significantly prolonged the atrial effective refractory period during vagal stimulation in their in vivo canine study. Therefore, we believe that the dose of tertiapin (30 nmol/kg iv) used in the present study should be sufficient to block K_{ACh} channel current in vivo.

Second, data were obtained from anesthetized animals. Since the anesthesia would affect the autonomic tone, the results may not be directly applicable to conscious animals. However, because we cut and stimulated the right cardiac vagal nerve, changes in autonomic outflow associated with anesthesia might not have significantly affected the results.

Third, in the present study, we stimulated the vagal nerve according to binary white noise and a step-wise pattern, which was quite different from the pattern of physiological neuronal discharge. However, although nonphysiological patterns of stimulation could theoretically bias the system identification results, because coherence was near unity over the frequency range of interest, by virtue of their inherent linearity, the system properties would not vary much with differing patterns of stimulation.

In conclusion, K_{ACh} channel blockade with intravenous tertiapin administration decreased the dynamic gain and corner frequency without changing the lag time of the transfer function from vagal stimulation to HR. In the time domain, tertiapin prolonged the time constant and 90% rise time of the step response. Additionally, tertiapin decreased the static reductions of HR from baseline HR to less than half of the control response with increasing vagal stimulus frequency. These results suggest that K_{ACh} channels accelerate the dynamic HR response to vagal stimulation and contribute more to the static HR response for more potent tonic vagal stimulation in vivo.

Perspectives

To simply identify the role of K_{ACh} channels in vagal HR control, a previous study (34) and the present study completely and/or partially excluded background sympathetic tone. However, in the physiological condition, sympathetic tone affects vagal control of HR and vice versa [e.g., accentuated antagonism (17)]. Pathophysiological conditions such as chronic heart failure (25), hypertension (19), and obesity (30) reveal increased basal sympathetic nerve activity compared with the normal condition. Tertiapin did not affect basal AP or HR (Table 1), suggesting that tertiapin did not affect sympathetic tone in the present experimental settings. Furthermore, under β-adrenergic blockade (the supplemental protocol), tertiapin decreased the dynamic gain and corner frequency, suggesting that the effects of tertiapin cannot be explained by the background sympathetic tone. However, the experimental design of the present study did not allow separate assessment of the direct vs. the indirect action of ACh, because the indirect action of ACh was not manipulated intentionally. Further investigation is needed to clarify the effects of sympathetic tone on the contribution of K_{ACh} channels to negative chronotropic effects.

GRANTS

This study was supported by Health and Labour Sciences Research Grants H15-Physi-001, H18-Nano-Ippan-003, and H18-Iryo-Ippan-023 from the Ministry of Health, Grant-in-Aid for Scientific Research promoted by the Ministry of Education, Culture, Sports, Science and Technology in Japan 18591992, and the Ground-Based Research Announcement for Space Utilization project promoted by the Japan Space Forum. This study was also supported by Industrial Technology Research Program Grant 06B44524a from the New Energy and Industrial Technology Development Organization of Japan.

REFERENCES

1. **Bendat J, Piersol A.** Single-input/output relationships. In: *Random Data Analysis and Measurement Procedures* (3rd ed). New York: Wiley, 2000, p. 189–217.
2. **Berger RD, Saul JP, Cohen RJ.** Transfer function analysis of autonomic regulation. I. Canine atrial rate response. *Am J Physiol Heart Circ Physiol* 256: H142–H152, 1989.
3. **Breitwieser GE, Szabo G.** Uncoupling of cardiac muscarinic and β-adrenergic receptors from ion channels by a guanine nucleotide analogue. *Nature* 317: 538–540, 1985.
4. **Brigham E.** FFT transform application. In: *The Fast Fourier Transform and Its Application.* Englewood Cliffs, NJ: Prentice-Hall, 1988, p. 167–203.

5. **Dascal N, Schreibmayer W, Lim NF, Wang W, Chavkin C, DiMagno L, Labarca C, Kieffer BL, Gaveriaux-Ruff C, Trollinger D, Lester HA, Davidson N.** Atrial G protein-activated K^+ channel: expression, cloning, and molecular properties. *Proc Natl Acad Sci USA* 90: 10235–10239, 1993.
6. **DiFrancesco D.** Cardiac pacemaker: 15 years of "new" interpretation. *Acta Cardiol* 50: 413–427, 1995.
7. **Drici MD, Diochot S, Terrenoire C, Romey G, Lazdunski M.** The bee venom peptide tertiapin underlines the role of $I_{K\,ACh}$ in acetylcholine-induced atrioventricular blocks. *Br J Pharmacol* 131: 569–577, 2000.
8. **Gehrmann J, Meister M, Maguire CT, Martins DC, Hammer PE, Neer EJ, Berul CI, Mende U.** Impaired parasympathetic heart rate control in mice with a reduction of functional G protein βγ-subunits. *Am J Physiol Heart Circ Physiol* 282: H445–H456, 2002.
9. **Hartzell HC, Mery PF, Fischmeister R, Szabo G.** Sympathetic regulation of cardiac calcium current is due exclusively to cAMP-dependent phosphorylation. *Nature* 351: 573–576, 1991.
10. **Hashimoto N, Yamashita T, Tsuruzoe N.** Tertiapin, a selective $I_{K\,ACh}$ blocker, terminates atrial fibrillation with selective atrial effective refractory period prolongation. *Pharmacol Res* 54: 136–141, 2006.
11. **Huang CL, Slesinger PA, Casey PJ, Jan YN, Jan LY.** Evidence that direct binding of Gβγ to the GIRK1 G protein-gated inwardly rectifying K^+ channel is important for channel activation. *Neuron* 15: 1133–1143, 1995.
12. **Irisawa H, Brown HF, Giles W.** Cardiac pacemaking in the sinoatrial node. *Physiol Rev* 73: 197–227, 1993.
13. **Jin W, Lu Z.** Synthesis of a stable form of tertiapin: a high-affinity inhibitor for inward-rectifier K^+ channels. *Biochemistry* 38: 14286–14293, 1999.
14. **Kawada T, Ikeda Y, Sugimachi M, Shishido T, Kawaguchi O, Yamazaki T, Alexander J Jr, Sunagawa K.** Bidirectional augmentation of heart rate regulation by autonomic nervous system in rabbits. *Am J Physiol Heart Circ Physiol* 271: H288–H295, 1996.
15. **Kitamura H, Yokoyama M, Akita H, Matsushita K, Kurachi Y, Yamada M.** Tertiapin potently and selectively blocks muscarinic K^+ channels in rabbit cardiac myocytes. *J Pharmacol Exp Ther* 293: 196–205, 2000.
16. **Krapivinsky G, Gordon EA, Wickman K, Velimirovic B, Krapivinsky L, Clapham DE.** The G-protein-gated atrial K^+ channel $I_{K\,ACh}$ is a heteromultimer of two inwardly rectifying K^+-channel proteins. *Nature* 374: 135–141, 1995.
17. **Levy MN.** Sympathetic-parasympathetic interactions in the heart. *Circ Res* 29: 437–445, 1971.
18. **Luetje CW, Tietje KM, Christian JL, Nathanson NM.** Differential tissue expression and developmental regulation of guanine nucleotide binding regulatory proteins and their messenger RNAs in rat heart. *J Biol Chem* 263: 13357–13365, 1988.
19. **Mancia G, Grassi G, Giannattasio C, Seravalle G.** Sympathetic activation in the pathogenesis of hypertension and progression of organ damage. *Hypertension* 34: 724–728, 1999.
20. **Marmarelis P, Marmarelis V.** The white noise method in system identification. In: *Analysis of Physiological Systems*. New York: Plenum, 1978, p. 131–221.
21. **Miyamoto T, Kawada T, Takaki H, Inagaki M, Yanagiya Y, Jin Y, Sugimachi M, Sunagawa K.** High plasma norepinephrine attenuates the dynamic heart rate response to vagal stimulation. *Am J Physiol Heart Circ Physiol* 284: H2412–H2418, 2003.
22. **Miyamoto T, Kawada T, Yanagiya Y, Inagaki M, Takaki H, Sugimachi M, Sunagawa K.** Cardiac sympathetic nerve stimulation does not attenuate dynamic vagal control of heart rate via α-adrenergic mechanism. *Am J Physiol Heart Circ Physiol* 287: H860–H865, 2004.
23. **Nakahara T, Kawada T, Sugimachi M, Miyano H, Sato T, Shishido T, Yoshimura R, Miyashita H, Inagaki M, Alexander J Jr, Sunagawa K.** Accumulation of cAMP augments dynamic vagal control of heart rate. *Am J Physiol Heart Circ Physiol* 275: H562–H567, 1998.
24. **Nakahara T, Kawada T, Sugimachi M, Miyano H, Sato T, Shishido T, Yoshimura R, Miyashita H, Sunagawa K.** Cholinesterase affects dynamic transduction properties from vagal stimulation to heart rate. *Am J Physiol Regul Integr Comp Physiol* 275: R541–R547, 1998.
25. **Negrao CE, Rondon MU, Tinucci T, Alves MJ, Roveda F, Braga AM, Reis SF, Nastari L, Barretto AC, Krieger EM, Middlekauff HR.** Abnormal neurovascular control during exercise is linked to heart failure severity. *Am J Physiol Heart Circ Physiol* 280: H1286–H1292, 2001.
26. **Parker P, Celler BG, Potter EK, McCloskey DI.** Vagal stimulation and cardiac slowing. *J Auton Nerv Syst* 11: 226–231, 1984.
27. **Priola DV, Cote I.** Differential sensitivity of the canine heart to acetylcholine and vagal stimulation. *Am J Physiol Heart Circ Physiol* 234: H460–H464, 1978.
28. **Sakmann B, Noma A, Trautwein W.** Acetylcholine activation of single muscarinic K^+ channels in isolated pacemaker cells of the mammalian heart. *Nature* 303: 250–253, 1983.
29. **Saul JP, Berger RD, Albrecht P, Stein SP, Chen MH, Cohen RJ.** Transfer function analysis of the circulation: unique insights into cardiovascular regulation. *Am J Physiol Heart Circ Physiol* 261: H1231–H1245, 1991.
30. **Seals DR, Bell C.** Chronic sympathetic activation: consequence and cause of age-associated obesity? *Diabetes* 53: 276–284, 2004.
31. **Spear JF, Moore EN.** Influence of brief vagal and stellate nerve stimulation on pacemaker activity and conduction within the atrioventricular conduction system of the dog. *Circ Res* 32: 27–41, 1973.
32. **Sunahara RK, Dessauer CW, Gilman AG.** Complexity and diversity of mammalian adenylyl cyclases. *Annu Rev Pharmacol Toxicol* 36: 461–480, 1996.
33. **Wickman K, Nemec J, Gendler SJ, Clapham DE.** Abnormal heart rate regulation in GIRK4 knockout mice. *Neuron* 20: 103–114, 1998.
34. **Yamada M.** The role of muscarinic K^+ channels in the negative chronotropic effect of a muscarinic agonist. *J Pharmacol Exp Ther* 300: 681–687, 2002.
35. **Yamada M, Inanobe A, Kurachi Y.** G protein regulation of potassium ion channels. *Pharmacol Rev* 50: 723–760, 1998.

J Appl Physiol 102: 622–627, 2007.
First published November 2, 2006; doi:10.1152/japplphysiol.00622.2006.

Hypothermia reduces ischemia- and stimulation-induced myocardial interstitial norepinephrine and acetylcholine releases

Toru Kawada,[1] Hirotoshi Kitagawa,[2] Toji Yamazaki,[2] Tsuyoshi Akiyama,[2] Atsunori Kamiya,[1] Kazunori Uemura,[1] Hidezo Mori,[2] and Masaru Sugimachi[1]

[1]*Department of Cardiovascular Dynamics, Advanced Medical Engineering Center, and*
[2]*Department of Cardiac Physiology, National Cardiovascular Center Research Institute, Osaka, Japan*

Submitted 4 June 2006; accepted in final form 1 November 2006

Kawada T, Kitagawa H, Yamazaki T, Akiyama T, Kamiya A, Uemura K, Mori H, Sugimachi M. Hypothermia reduces ischemia- and stimulation-induced myocardial interstitial norepinephrine and acetylcholine releases. *J Appl Physiol* 102: 622–627, 2007. First published November 2, 2006; doi:10.1152/japplphysiol.00622.2006.—Although hypothermia is one of the most powerful modulators that can reduce ischemic injury, the effects of hypothermia on the function of the cardiac autonomic nerves in vivo are not well understood. We examined the effects of hypothermia on the myocardial interstitial norepinephrine (NE) and ACh releases in response to acute myocardial ischemia and to efferent sympathetic or vagal nerve stimulation in anesthetized cats. We induced acute myocardial ischemia by coronary artery occlusion. Compared with normothermia ($n = 8$), hypothermia at 33°C ($n = 6$) suppressed the ischemia-induced NE release [63 nM (SD 39) vs. 18 nM (SD 25), $P < 0.01$] and ACh release [11.6 nM (SD 7.6) vs. 2.4 nM (SD 1.3), $P < 0.01$] in the ischemic region. Under hypothermia, the coronary occlusion increased the ACh level from 0.67 nM (SD 0.44) to 6.0 nM (SD 6.0) ($P < 0.05$) and decreased the NE level from 0.63 nM (SD 0.19) to 0.40 nM (SD 0.25) ($P < 0.05$) in the nonischemic region. Hypothermia attenuated the nerve stimulation-induced NE release from 1.05 nM (SD 0.85) to 0.73 nM (SD 0.73) ($P < 0.05$, $n = 6$) and ACh release from 10.2 nM (SD 5.1) to 7.1 nM (SD 3.4) ($P < 0.05$, $n = 5$). In conclusion, hypothermia attenuated the ischemia-induced NE and ACh releases in the ischemic region. Moreover, hypothermia also attenuated the nerve stimulation-induced NE and ACh releases. The Bezold-Jarisch reflex evoked by the left anterior descending coronary artery occlusion, however, did not appear to be affected under hypothermia.

vagal nerve; sympathetic nerve; cardiac microdialysis; cats

HYPOTHERMIA IS ONE OF THE most powerful modulators that can reduce ischemic injury in the central nervous system, heart, and other organs. The general consensus is that hypothermia induces a hypometabolic state in tissues and balances energy supply and demand (25). With respect to the myocardial ischemia, the size of a myocardial infarction correlates with temperature (6), and mild hypothermia can protect the myocardium against acute ischemic injury (9). The effects of hypothermia on the function of the cardiac autonomic nerves in terms of neurotransmitter releases, however, are not fully understood. Because autonomic neurotransmitters such as norepinephrine (NE) and ACh directly impinge on the myocardium, they would be implicated in the cardioprotection by hypothermia.

In previous studies from our laboratory, Kitagawa et al. (16) demonstrated that hypothermia attenuated the nonexocytotic NE release induced pharmacologically by ouabain, tyramine, or cyanide. Kitagawa et al. (15) also demonstrated that hypothermia attenuated the exocytotic NE release in response to vena cava occlusion or to local administration of high K^+. The effects of hypothermia on the ischemia-induced myocardial interstitial NE release, however, were not examined in those studies. In addition, the effects of hypothermia on the ischemia-induced myocardial interstitial ACh release have never been examined. Because both sympathetic and parasympathetic nerves control the heart, simultaneous monitoring of the myocardial interstitial releases of NE and ACh (14, 31) would help integrative understanding of the autonomic nerve terminal function under hypothermia in conjunction with acute myocardial ischemia.

In the present study, the effects of hypothermia on the ischemia-induced and nerve stimulation-induced myocardial interstitial neurotransmitter releases were examined. We implanted a dialysis probe into the left ventricular free wall of anesthetized cats and measured dialysate NE and ACh levels as indexes of neurotransmitter outputs from the cardiac sympathetic and vagal nerve terminals, respectively. Based on our laboratory's previous results (15, 16), we hypothesized that hypothermia would attenuate the neurotransmitter releases in response to acute myocardial ischemia and to electrical nerve stimulation.

MATERIALS AND METHODS

Surgical Preparation and Protocols

Animals were cared for in accordance with the *Guiding Principles for the Care and Use of Animals in the Field of Physiological Sciences*, approved by the Physiological Society of Japan. All protocols were reviewed and approved by the Animal Subjects Committee of National Cardiovascular Center. Adult cats were anesthetized via an intraperitoneal injection of pentobarbital sodium (30–35 mg/kg) and ventilated mechanically through an endotracheal tube with oxygen-enriched room air. The level of anesthesia was maintained with a continuous intravenous infusion of pentobarbital sodium (1–2 $mg \cdot kg^{-1} \cdot h^{-1}$) through a catheter inserted from the right femoral vein. Mean arterial pressure (MAP) was measured using a pressure transducer connected to a catheter inserted from the right femoral artery. Heart rate (HR) was determined from an electrocardiogram.

Protocol 1: acute myocardial ischemia. We examined the effects of hypothermia on the ischemia-induced myocardial interstitial releases of NE and ACh. The heart was exposed by partially removing the left fifth and/or sixth rib. A dialysis probe was implanted transversely into

Address for reprint requests and other correspondence: T. Kawada, Dept. of Cardiovascular Dynamics, Advanced Medical Engineering Center, National Cardiovascular Center Research Institute, 5-7-1 Fujishirodai, Suita, Osaka 565-8565, Japan (e-mail: torukawa@res.ncvc.go.jp).

The costs of publication of this article were defrayed in part by the payment of page charges. The article must therefore be hereby marked "*advertisement*" in accordance with 18 U.S.C. Section 1734 solely to indicate this fact.

the anterolateral free wall of the left ventricle perfused by the left anterior descending coronary artery (LAD) to monitor myocardial interstitial NE and ACh levels in the ischemic region during occlusion of the LAD (13). Another dialysis probe was implanted transversely into the posterior free wall of the left ventricle perfused by the left circumflex coronary artery to monitor myocardial interstitial NE and ACh levels in a nonischemic region. Heparin sodium (100 U/kg) was administered intravenously to prevent blood coagulation. Animals were divided into a normothermic group (n = 8) and a hypothermic group (n = 6). In the hypothermic group, surface cooling with ice bags was performed until the esophageal temperature decreased to 33°C (15, 16). A stable hypothermic condition was obtained within ~2 h. In each group, we occluded the LAD for 60 min and examined changes in the myocardial interstitial NE and ACh levels in the ischemic region (i.e., the LAD region) and nonischemic region (i.e., the left circumflex coronary artery region). Fifteen-minute dialysate samples were obtained during the preocclusion baseline condition and during the periods of 0–15, 15–30, 30–45, and 45–60 min of the LAD occlusion.

Protocol 2: sympathetic stimulation. We examined the effects of hypothermia on the sympathetic nerve stimulation-induced myocardial interstitial NE release (n = 6). A dialysis probe was implanted transversely into the anterolateral free wall of the left ventricle. The bilateral cardiac sympathetic nerves originating from the stellate ganglia were exposed through a second intercostal space and sectioned. The cardiac end of each sectioned nerve was placed on a bipolar platinum electrode for sympathetic stimulation (5 Hz, 10 V, 1-ms pulse duration). The electrodes and nerves were covered with mineral oil to provide insulation and prevent desiccation. A 4-min dialysate sample was obtained during the sympathetic stimulation under the normothermic condition. Thereafter, hypothermia was introduced using the same cooling procedure as in *protocol 1*, and a second 4-min dialysate sample was obtained during the sympathetic stimulation.

Protocol 3: vagal stimulation. We examined the effects of hypothermia on the vagal nerve stimulation-induced ACh release (n = 5). A dialysis probe was implanted transversely into the anterolateral free wall of the left ventricle. The bilateral vagi were exposed through a midline cervical incision and sectioned at the neck. The cardiac end of each sectioned nerve was placed on a bipolar platinum electrode for vagal stimulation (20 Hz, 10 V, 1-ms pulse duration). To prevent severe bradycardia and cardiac arrest, which can be induced by the vagal stimulation, the heart was paced at 200 beats/min using pacing wires attached to the apex of the heart during the stimulation period. A 4-min dialysate sample was obtained during the vagal stimulation under the normothermic condition. Thereafter, hypothermia was introduced using the same cooling procedure as in *protocol 1*, and a second 4-min dialysate sample was obtained during the vagal stimulation.

Because of the relatively intense stimulation of the sympathetic or vagal nerve, the stimulation period in *protocols 2* and *3* was limited to 4 min to minimize gradual waning of the stimulation effects. At the end of the experiment, the animals were killed by increasing the depth of anesthesia with an overdose of pentobarbital sodium. We then confirmed that the dialysis probes had been threaded in the middle layer of the left ventricular myocardium.

Dialysis Technique

The dialysate NE and ACh concentrations were measured as indexes of myocardial interstitial NE and ACh levels, respectively. The materials and properties of the dialysis probe have been described previously (2, 3). Briefly, we designed a transverse dialysis probe. A dialysis fiber (13-mm length, 310-μm outer diameter, 200-μm inner diameter; PAN-1200, 50,000 molecular weight cutoff; Asahi Chemical) was connected at both ends to polyethylene tubes (25-cm length, 500-μm outer diameter, 200-μm inner diameter). The dialysis probe was perfused with Ringer solution containing a cholinesterase inhibitor eserine (10^{-4} M) at a rate of 2 μl/min. We started dialysate sampling from 2 h after the implantation of the dialysis probe(s), when the dialysate NE and ACh concentrations had reached steady states. The actual dialysate sampling was delayed by 5 min from the collection period to account for the dead space volume between the semipermeable membrane and the sample tube. Each sample was collected in a microtube containing 3 μl of HCl to prevent amine oxidation. The dialysate ACh concentration was measured directly by HPLC with electrochemical detection (Eicom). The in vitro recovery rate of ACh was ~70%. With the use of a criterion of signal-to-noise ratio of higher than three, the detection limit for ACh was 3 pg per injection. The dialysate NE concentration was measured by another HPLC-electrochemical detection system after the removal of interfering compounds by an alumina procedure. The in vitro recovery rate of NE was ~55%. With the use of a criterion of signal-to-noise ratio of higher than three, the detection limit for NE was 200 fg per injection.

Statistical Analysis

All data are presented as means and SD values. For *protocol 1*, we performed two-way repeated-measures ANOVA using hypothermia as one factor and the dialysate sampling periods (the effects of ischemia) as the other factor. For *protocols 2* and *3*, we compared stimulation-induced releases of NE and ACh before and during hypothermia using a paired t-test. For all of the statistics, the difference was considered significant when $P < 0.05$.

RESULTS

Figure 1*A* illustrates changes in myocardial interstitial NE levels in the ischemic region during LAD occlusion obtained from *protocol 1*. The *inset* shows the magnified ordinate for the

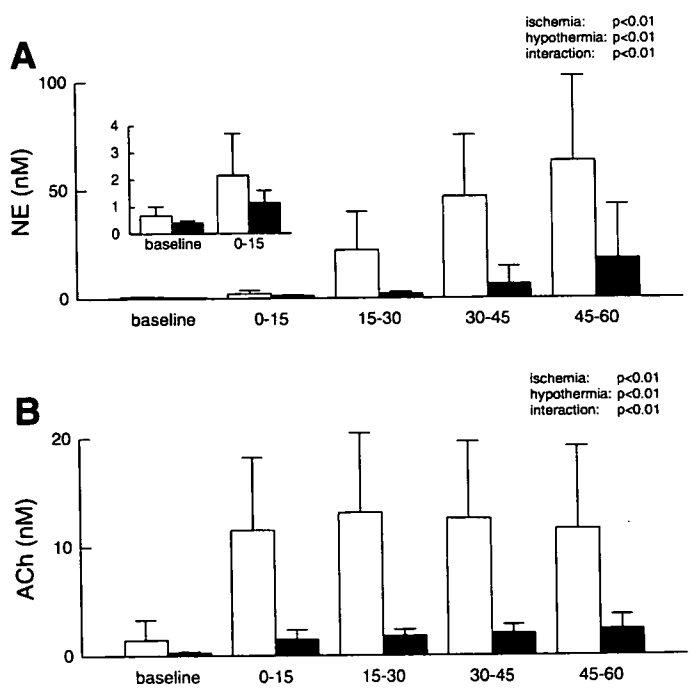

Fig. 1. *A*: ischemia-induced myocardial interstitial norepinephrine (NE) release in the ischemic region. Acute myocardial ischemia caused a progressive increase in the level of myocardial interstitial NE. Hypothermia attenuated the ischemia-induced NE release. *Inset*: magnified ordinate for the baseline and the 0- to 15-min period of ischemia. *B*: ischemia-induced myocardial interstitial ACh release in the ischemic region. Acute myocardial ischemia increased the myocardial interstitial ACh levels. Hypothermia attenuated the ischemia-induced ACh release. Open bars: normothermia; solid bars: hypothermia.

baseline and the 0- to 15-min period of ischemia. In the normothermic group (open bars), the LAD occlusion caused an ~94-fold increase in the NE level during the 45- to 60-min interval. In the hypothermic group (solid bars), the LAD occlusion caused an ~45-fold increase in the NE level during the 45- to 60-min interval. Compared with normothermia, hypothermia suppressed the baseline NE level to ~59% and the NE level during the 45- to 60-min period to ~29%. Statistical analysis indicated that the effects of both hypothermia and ischemia on the NE release were significant, and the interaction between hypothermia and ischemia was also significant.

Figure 1*B* illustrates changes in myocardial interstitial ACh levels in the ischemic region during the LAD occlusion. In both the normothermic (open bars) and hypothermic (solid bars) groups, the LAD occlusion caused an approximately eightfold increase in the ACh level during the 45- to 60-min interval. Compared with normothermia, however, hypothermia suppressed both the baseline ACh level and the ACh level during the 45- to 60-min period of ischemia to ~20%. Statistical analysis indicated that the effects of both hypothermia and ischemia on the ACh release were significant, and the interaction between hypothermia and ischemia was also significant.

Figure 2*A* illustrates changes in myocardial interstitial NE levels in the nonischemic region during the LAD occlusion. Note that scale of the ordinate is only one-hundredth of that in Fig. 1*A*. The LAD occlusion decreased the NE level in the normothermic group (open bars); the NE level during the 45- to 60-min interval was ~59% of the baseline level. The LAD occlusion also decreased the NE level in the hypothermic group (solid bars); the NE level during the 45- to 60-min interval was ~64% of the baseline level. Although the LAD occlusion resulted in a decrease in the NE level under both conditions, the NE level under hypothermia was nearly twice that measured under normothermia. The statistical analysis indicated that the effects of both hypothermia and ischemia on the NE release were significant, whereas the interaction between hypothermia and ischemia was not significant.

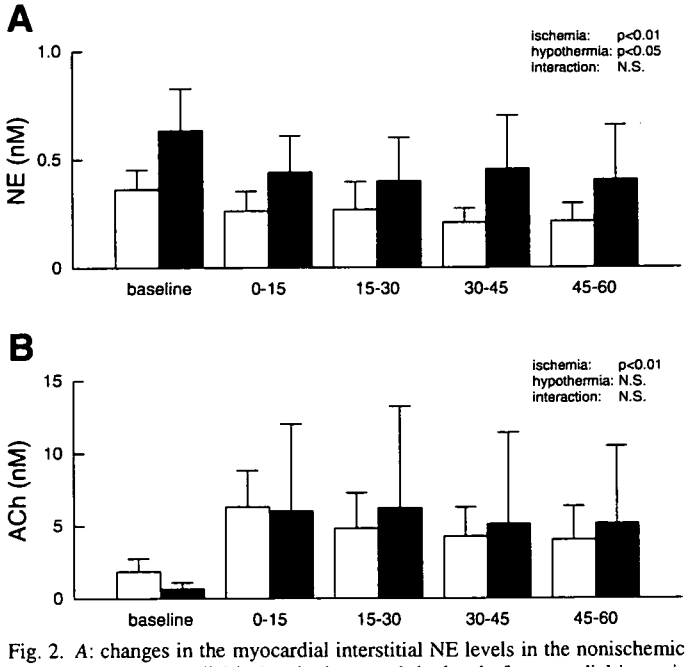

Fig. 2. *A*: changes in the myocardial interstitial NE levels in the nonischemic region. Acute myocardial ischemia decreased the level of myocardial interstitial NE from the baseline level. Hypothermia increased the myocardial interstitial NE levels in the nonischemic region. *B*: changes in the myocardial interstitial ACh levels in the nonischemic region. Acute myocardial ischemia increased the myocardial interstitial ACh level. Hypothermia did not attenuate the increasing response of ACh to the left anterior descending coronary artery occlusion. Open bars: normothermia; solid bars: hypothermia. NS, not significant.

Table 1. *Mean arterial pressure during acute myocardial ischemia obtained in protocol 1*

	Baseline	5 min	15 min	30 min	45 min	60 min
Normothermia	108 (23)	102 (28)	101 (24)	101 (20)	102 (21)	102 (21)
Hypothermia	108 (11)	80 (17)	87 (10)	85 (10)	86 (10)	91 (11)

Values are means (SD) (in mmHg) obtained during preocclusion baseline period and 5-, 15-, 30-, 45-, and 60-min periods of coronary artery occlusion. Ischemia: $P < 0.01$; hypothermia: not significant; interaction: $P < 0.01$.

Figure 2*B* illustrates changes in myocardial interstitial ACh levels in the nonischemic region during the LAD occlusion. The LAD occlusion caused an ~3.4-fold increase in the ACh level during the 0- to 15-min interval in the normothermic group (open bars). The LAD occlusion caused an approximately ninefold increase in the ACh level during the 0- to 15-min interval in the hypothermic group (solid bars). These effects of ischemia on the ACh release were statistically significant. Although hypothermia seemed to attenuate the baseline ACh level, the overall effects of hypothermia on the ACh level were insignificant.

Tables 1 and 2 summarize the MAP and HR data, respectively, obtained in *protocol 1*. Acute myocardial ischemia significantly reduced MAP ($P < 0.01$) and HR ($P < 0.01$). Hypothermia did not affect MAP but did decrease HR ($P < 0.01$). The interaction between ischemia and hypothermia was significant for MAP but not for HR by the two-way repeated-measures ANOVA.

For *protocol 2*, hypothermia significantly attenuated the sympathetic stimulation-induced NE release to ~70% of the level observed during normothermia (Fig. 3*A*). Under normothermia, the sympathetic stimulation increased MAP from 114 mmHg (SD 27) to 134 mmHg (SD 33) ($P < 0.01$) and HR from 147 beats/min (SD 9) to 207 beats/min (SD 5) ($P < 0.01$). Under hypothermia, the sympathetic stimulation increased MAP from 117 mmHg (SD 11) to 136 mmHg (SD 22) ($P < 0.05$) and HR from 125 beats/min (SD 16) to 164 beats/min (SD 10) ($P < 0.01$).

For *protocol 3*, hypothermia significantly attenuated the vagal stimulation-induced ACh release to ~70% of the level observed during normothermia (Fig. 3*B*). Hypothermia did not change MAP [117 mmHg (SD 18) vs. 118 mmHg (SD 27)] but

Table 2. *Heart rate during acute myocardial ischemia obtained in protocol 1*

	Baseline	5 min	15 min	30 min	45 min	60 min
Normothermia	183 (26)	160 (18)	163 (16)	163 (18)	166 (20)	165 (21)
Hypothermia	146 (25)	116 (19)	113 (19)	126 (39)	112 (20)	97 (31)

Values are means (SD) (in beats/min) obtained during preocclusion baseline period and 5-, 15-, 30-, 45-, and 60-min periods of coronary artery occlusion. Ischemia: $P < 0.01$; hypothermia: $P < 0.01$; interaction: not significant.

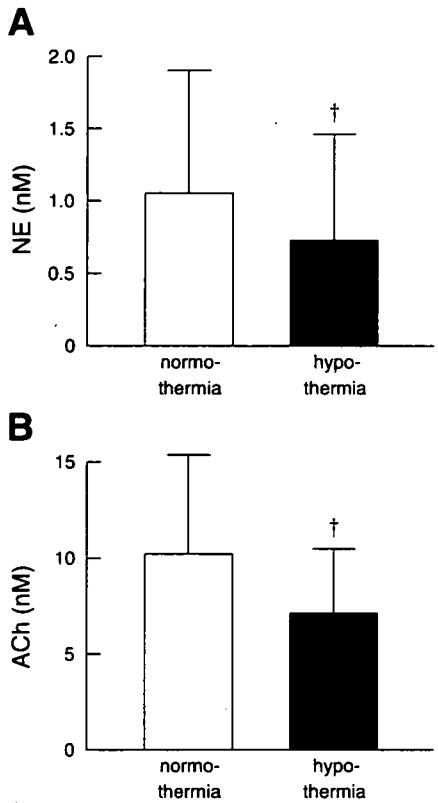

Fig. 3. *A*: efferent sympathetic nerve stimulation-induced release of myocardial interstitial NE before and during hypothermia. †Hypothermia significantly attenuated the stimulation-induced NE release. *B*: efferent vagal nerve stimulation-induced release of myocardial interstitial ACh before and during hypothermia. †Hypothermia significantly attenuated the stimulation-induced ACh release.

did decrease HR from 202 beats/min (SD 24) to 179 beats/min (SD 15) ($P < 0.05$) during the prestimulation, unpaced condition. MAP during the stimulation was 105 mmHg (SD 19) under normothermia and 93 mmHg (SD 33) under hypothermia.

DISCUSSION

A cardiac microdialysis is a powerful tool to estimate neurotransmitter levels in the myocardial interstitium in vivo (2, 3, 14, 19, 20, 31). The present study demonstrated that hypothermia significantly attenuated the myocardial interstitial releases of NE and ACh in the ischemic region during the LAD occlusion. In contrast, the increasing response in the ACh level from its baseline level and the decreasing response in the NE level from its baseline level observed in the nonischemic region were maintained under hypothermia. To our knowledge, this is the first report showing the effects of hypothermia on the myocardial interstitial releases of NE and ACh during acute myocardial ischemia in vivo. In addition, the present study showed that hypothermia significantly attenuated nerve stimulation-induced myocardial interstitial NE and ACh releases in vivo.

Effects of Hypothermia on Ischemia-induced NE and ACh Releases in the Ischemic Region

Acute myocardial ischemia causes energy depletion, which leads to myocardial interstitial NE release in the ischemic region (Fig. 1*A*). The NE release can be classified as exocytotic or nonexocytotic (18, 24). Exocytotic release indicates NE release from synaptic vesicles, which normally occurs in response to nerve discharge and subsequent Ca^{2+} influx through voltage-dependent Ca^{2+} channels. On the other hand, nonexocytotic release indicates NE release from the axoplasm, such as that mediated by a reverse transport through the NE transporter. A neuronal uptake blocker, desipramine, can suppress the ischemia-induced NE release (19, 24). Whereas exocytotic release contributes to the ischemia-induced NE release in the initial phase of ischemia (within ~20 min), carrier-mediated nonexocytotic release becomes predominant as the ischemic period is prolonged (1). Hypothermia significantly attenuated the ischemia-induced NE release (Fig. 1*A*). The NE level during the 45- to 60-min period of ischemia under hypothermia was ~20% of that obtained under normothermia. The NE uptake transporter is driven by the Na^+ gradient across the cell membrane (23). The loss of the Na^+ gradient due to ischemia causes NE to be transported out of the cell by reversing the action of the NE transporter. Hypothermia inhibits the action of the NE transporter and also suppresses the intracellular Na^+ accumulation (8), thereby reducing nonexocytotic NE release during ischemia. The present results are in line with an in vitro study that showed hypothermia suppressed nonexocytotic NE release induced by deprivation of oxygen and glucose (30). The present results are also consistent with a previous study from our laboratory that showed hypothermia attenuated the nonexocytotic NE release induced by ouabain, tyramine, or cyanide (16).

Acute myocardial ischemia increases myocardial interstitial ACh level in the ischemic region, as reported previously (Fig. 1*B*) (13). The level of ischemia-induced ACh release during 0- to 15-, 15- to 30-, 30- to 45-, or 45- to 60-min period of ischemia is comparable to that evoked by 4-min electrical stimulation of the bilateral vagi (Fig. 3*B*). Compared with the normothermic condition, hypothermia significantly attenuated the ischemia-induced myocardial interstitial release of ACh in the ischemic region. Our laboratory's previous study indicated that intracellular Ca^{2+} mobilization is essential for the ischemia-induced release of ACh (13). Hypothermia may have prevented the Ca^{2+} overload, thereby reducing the ischemia-induced ACh release. Alternatively, hypothermia may reduce the extent of the ischemic injury, which in turn suppressed the ischemia-induced ACh release. Because ACh has protective effects on the cardiomyocytes against ischemia (11), the suppression of ischemia-induced ACh release during hypothermia itself may be unfavorable for cardioprotection.

There is considerable controversy regarding the cardioprotective effects of β-adrenergic blockade during severe ischemia, with studies demonstrating a reduction of infarct size (10, 17) or no effects (7, 27). The β-adrenergic blockade seems effective to protect the heart only when the heart is reperfused within a certain period after the coronary occlusion. The β-adrenergic blockade would reduce the myocardial oxygen consumption through the reduction of HR and ventricular contractility and delay the progression of ischemic injury. Hence the infarct size might be reduced when the heart is reperfused before the ischemic damage becomes irreversible. The ischemia-induced NE release reached nearly 100 times the baseline NE level under normothermia (Fig. 1*A*), which by far exceeded the NE level attained by electrical stimulation of the

bilateral stellate ganglia (Fig. 3*A*). Because high NE levels have cardiotoxic effects (22), ischemia-induced NE release might aggravate the ischemic injury. However, catecholamine depletion by a reserpine treatment fails to reduce the infarct size (26, 29), throwing a doubt on the involvement of catecholamine toxicity in the progression of myocardial damage during ischemia. It is, therefore, most likely that the hypothermia-induced reductions in NE and ACh are the result of reduced myocardial damage or a direct effect on nerve endings.

Van den Doel et al. (28) showed that hypothermia does not abolish necrosis, but rather delays necrosis during sustained ischemia, so that hypothermia protected against infarction produced by a 30-min occlusion but not against infarction produced by a 60-min occlusion in the rat heart. At the same time, they mentioned that hypothermia was able to reduce the infarct size after a 60-min coronary occlusion in the dog, possibly because of the significant collateral flow in the canine hearts. Because the feline hearts are similar to the canine hearts in that they have considerable collateral flow compared with the rat hearts (21), hypothermia should have protected the feline heart against the 60-min coronary occlusion in the present study.

Effects of Hypothermia on the NE and ACh Releases in the Nonischemic Region and on the Electrical Stimulation-induced NE and ACh Releases

The NE and ACh levels in the nonischemic region may reflect the sympathetic and parasympathetic drives to this region. As an example, myocardial interstitial ACh levels increase during activations of the arterial baroreflex and the Bezold-Jarisch reflex (14). In the present study, acute myocardial ischemia decreased the NE level from its baseline level, whereas it increased the ACh level from its baseline level (Fig. 2). Ischemia also decreased MAP and HR (Tables 1 and 2), suggesting that the Bezold-Jarisch reflex was induced by the LAD occlusion under both normothermia and hypothermia. Taking into account the fact that electrical stimulation-induced ACh release was attenuated to ~70% (Fig. 3), similar ACh levels during ischemia imply the enhancement of the parasympathetic outflow via the Bezold-Jarisch reflex under hypothermia. These results are in line with the study by Zheng et al. (32), where pulmonary chemoreflex-induced bradycardia was maintained under hypothermia. Hypothermia increased the NE level in the nonischemic region, suggesting that sympathetic drive to this region also increased. Hypothermic stress is known to cause sympathetic activation, accompanying increases in MAP, HR, plasma NE, and epinephrine levels (4). In the present study, because the effect of hypothermia on MAP was insignificant (Table 1) and HR decreased under hypothermia (Table 2), the sympathetic activation observed in the nonischemic region might have been regional and not systemic.

Hypothermia attenuated the releases of NE and ACh in response to respective nerve stimulation to ~70% of that observed under normothermia (Fig. 3). The suppression of the exocytotic NE release by hypothermia is consistent with a previous study from our laboratory, where hypothermia attenuated the myocardial interstitial NE release in response to vena cava occlusion or to a local high K^+ administration (15). The suppression of NE release by hypothermia is consistent with an in vitro study by Kao and Westhead (12) in which catecholamine secretion from adrenal chromaffin cells induced by elevated K^+ levels increased as the temperature increased from 4 to 37°C. On the other hand, because hypothermia inhibits the neuronal NE uptake, the NE concentration at the synaptic cleft is expected to be increased if the level of NE release remains unchanged. Actually, Vizi (30) demonstrated that hypothermia increased NE release in response to field stimulation in vitro. In the present study, however, the suppression of NE release might have canceled the potential accumulation of NE due to NE uptake inhibition. The present study also demonstrated that the ACh release was suppressed by hypothermia. In the rat striatum, hypothermia decreases the extracellular ACh concentration and increases the choline concentration (5). Hypothermia may inhibit a choline uptake transporter in the same manner as it inhibits a NE uptake transporter. The inhibition of the choline transporter by hypothermia may have hampered the replenishment of the available pool of ACh and thereby contributed to the suppression of the stimulation-induced ACh release.

Limitations

In *protocol 1*, because we did not measure the infarct size in the present study, the degree of myocardial protection by hypothermia was undetermined. Whether the reduction of ischemia-induced neurotransmitter release correlates with the reduction of infact size requires further investigations. In *protocols 2* and *3*, baseline NE and ACh levels were not measured. The reduction of stimulation-induced NE and ACh release by hypothermia might be partly due to the reduction of baseline NE and ACh levels. However, because transection of the stellate ganglia (31) or vagi (3) reduces the baseline NE and ACh levels, changes in the baseline NE and ACh levels by hypothermia in *protocols 2* and *3* could not be as large as those observed under innervated conditions in *protocol 1* (Figs. 1 and 2).

In conclusion, hypothermia attenuated the ischemia-induced releases of NE and ACh in the ischemic region to ~30 and 20% of those observed under normothermia, respectively. Hypothermia also attenuated the nerve stimulation-induced releases of NE and ACh to ~70% of those observed during normothermia. In contrast, hypothermia did not affect the decreasing response in the NE level and the increasing response in the ACh level in the nonischemic region, suggesting that the Bezold-Jarisch reflex evoked by the LAD occlusion was maintained.

GRANTS

This study was supported by Health and Labour Sciences Research Grant for Research on Advanced Medical Technology, Health and Labour Sciences Research Grant for Research on Medical Devices for Analyzing, Supporting and Substituting the Function of Human Body, and Health and Labour Sciences Research Grant H18-Iryo-Ippan-023 from the Ministry of Health, Labour and Welfare of Japan; Program for Promotion of Fundamental Studies in Health Science from the National Institute of Biomedical Innovation; a grant provided by the Ichiro Kanehara Foundation; Ground-based Research Announcement for Space Utilization promoted by the Japan Space Forum; and Industrial Technology Research Grant Program 03A47075 from the New Energy and Industrial Technology Development Organization of Japan.

REFERENCES

1. **Akiyama T, Yamazaki T.** Norepinephrine release from cardiac sympathetic nerve endings in the in vivo ischemic region. *J Cardiovasc Pharmacol* 34: S11–S14, 1999.

2. **Akiyama T, Yamazaki T, Ninomiya I.** In vivo monitoring of myocardial interstitial norepinephrine by dialysis technique. *Am J Physiol Heart Circ Physiol* 261: H1643–H1647, 1991.
3. **Akiyama T, Yamazaki T, Ninomiya I.** In vivo detection of endogenous acetylcholine release in cat ventricles. *Am J Physiol Heart Circ Physiol* 266: H854–H860, 1994.
4. **Chernow B, Lake CR, Zaritsky A, Finton CK, Casey L, Rainey TG, Fletcher JR.** Sympathetic nervous system "switch off" with severe hypothermia. *Crit Care Med* 11: 677–680, 1983.
5. **Damsma G, Fibiger HC.** The effects of anaesthesia and hypothermia on interstitial concentrations of acetylcholine and choline in rat striatum. *Life Sci* 48: 2469–2474, 1991.
6. **Duncker DJ, Klassen CL, Ishibashi Y, Herrlinger SH, Pavek T, Bache R.** Effect of temperature on myocardial infarction in swine. *Am J Physiol Heart Circ Physiol* 270: H1189–H1199, 1996.
7. **Genth K, Hofmann M, Hofmann M, Schaper W.** The effect of β-adrenergic blockade on infarct size following experimental coronary occlusion. *Basic Res Cardiol* 76: 144–151, 1981.
8. **Gerevich Z, Tretter L, Adam-Vizi V, Baranyi M, Kiss JP, Zelles T, Vizi ES.** Analysis of high intracellular [Na^+]-induced release of [^{3}H]noradrenaline in rat hippocampal slices. *Neuroscience* 104: 761–768, 2001.
9. **Hale SL, Kloner RA.** Myocardial temperature in acute myocardial infarction: protection with mild regional hypothermia. *Am J Physiol Heart Circ Physiol* 273: H220–H227, 1997.
10. **Jang IK, Van de Werf F, Vanhaecke J, De Geest H.** Coronary reperfusion by thrombolysis and early beta-adrenergic blockade in acute experimental myocardial infarction. *J Am Coll Cardiol* 14: 1816–1823, 1989.
11. **Kakinuma Y, Ando M, Kuwabara M, Katare RG, Okudela K, Kobayashi M, Sato T.** Acetylcholine from vagal stimulation protects cardiomyocytes against ischemia and hypoxia involving additive nonhypoxic induction of HIF-1α. *FEBS Lett* 579: 2111–2118, 2005.
12. **Kao LS, Westhead EW.** Temperature dependence of catecholamine secretion from cultured bovine chromaffin cells. *J Neurochem* 43: 590–592, 1984.
13. **Kawada T, Yamazaki T, Akiyama T, Sato T, Shishido T, Inagaki M, Takaki H, Sugimachi M, Sunagawa K.** Differential acetylcholine release mechanisms in the ischemic and non-ischemic myocardium. *J Mol Cell Cardiol* 32: 405–414, 2000.
14. **Kawada T, Yamazaki T, Akiyama T, Shishido T, Inagaki M, Uemura K, Miyamoto T, Sugimachi M, Takaki H, Sunagawa K.** In vivo assessment of acetylcholine-releasing function at cardiac vagal nerve terminals. *Am J Physiol Heart Circ Physiol* 281: H139–H145, 2001.
15. **Kitagawa H, Akiyama T, Yamazaki T.** Effects of moderate hypothermia on in situ cardiac sympathetic nerve endings. *Neurochem Int* 40: 235–242, 2002.
16. **Kitagawa H, Yamazaki T, Akiyama T, Mori H, Sunagawa K.** Effects of moderate hypothermia on norepinephrine release evoked by ouabain, tyramine and cyanide. *J Cardiovasc Pharmacol* 41: S111–S114, 2003.
17. **Ku DD, Lucchesi BR.** Effects of dimethyl propranolol (UM-272; SC-27761) on myocardial ischemic injury in the canine heart after temporary coronary artery occlusion. *Circulation* 57: 541–548, 1978.
18. **Kurz T, Richardt G, Hagl S, Seyfarth M, Schömig A.** Two different mechanisms of noradrenaline release during normoxia and simulated ischemia in human cardiac tissue. *J Mol Cell Cardiol* 27: 1161–1172, 1995.
19. **Lameris TW, de Zeeuw S, Alberts G, Boomsma F, Duncker DJ, Verdouw PD, Veld AJ, van den Meiracker AH.** Time course and mechanism of myocardial catecholamine release during transient ischemia in vivo. *Circulation* 101: 2645–2650, 2000.
20. **Lameris TW, de Zeeuw S, Duncker DJ, Alberts G, Boomsma F, Verdouw PD, van den Meiracker AH.** Exogenous angiotensin II does not facilitate norepinephrine release in the heart. *Hypertension* 40: 491–497, 2002.
21. **Maxwell MP, Hearse DJ, Yellon DM.** Species variation in the coronary collateral circulation during regional myocardial ischaemia: a critical determinant of the rate of evolution and extent of myocardial infarction. *Cardiovasc Res* 21: 737–746, 1987.
22. **Rona G.** Catecholamine cardiotoxicity. *J Mol Cell Cardiol* 17: 291–306, 1985.
23. **Schwartz JH.** Neurotransmitters. In: *Principles of Neural Science* (4th Ed.), edited by Kandel ER, Schwartz JH, Jessell TM. New York: McGraw-Hill, 2000, p. 280–297.
24. **Schömig A, Kurz T, Richardt G, Schömig E.** Neuronal sodium homeostasis and axoplasmic amine concentration determine calcium-independent noradrenaline release in normoxic and ischemic rat heart. *Circ Res* 63: 214–226, 1988.
25. **Simkhovich BZ, Hale SL, Kloner RA.** Metabolic mechanism by which mild regional hypothermia preserves ischemic tissue. *J Cardiovasc Pharmacol Ther* 9: 83–90, 2004.
26. **Toombs CF, Wiltse AL, Shebuski RJ.** Ischemic preconditioning fails to limit infarct size in reserpinized rabbit myocardium. Implication of norepinephrine release in the preconditioning effect. *Circulation* 88: 2351–2358, 1993.
27. **Torr S, Drake-Holland AJ, Main M, Hynd J, Isted K, Noble MIM.** Effects on infarct size of reperfusion and pretreatment with β-blockade and calcium antagonists. *Basic Res Cardiol* 84: 564–582, 1989.
28. **Van den Doel MA, Gho BC, Duval SY, Schoemaker RG, Duncker DJ, Verdouw PD.** Hypothermia extends the cardioprotection by ischaemic preconditioning to coronary artery occlusions of longer duration. *Cardiovasc Res* 37: 76–81, 1998.
29. **Vander Heide RS, Schwartz LM, Jennings RB, Reimer KA.** Effect of catecholamine depletion on myocardial infarct size in dogs: role of catecholamines in ischemic preconditioning. *Cardiovasc Res* 30: 656–662, 1995.
30. **Vizi ES.** Different temperature dependence of carrier-mediated (cytoplasmic) and stimulus-evoked (exocytotic) release of transmitter: a simple method to separate the two types of release. *Neurochem Int* 33: 359–366, 1998.
31. **Yamazaki T, Akiyama T, Kitagawa H, Takauchi Y, Kawada T, Sunagawa K.** A new, concise dialysis approach to assessment of cardiac sympathetic nerve terminal abnormalities. *Am J Physiol Heart Circ Physiol* 272: H1182–H1187, 1997.
32. **Zheng F, Kidd C, Bowser-Riley F.** Effects of moderate hypothermia on baroreflex and pulmonary chemoreflex heart rate response in decerebrate ferrets. *Exp Physiol* 81: 409–420, 1996.